Regional dependence in the timing of onset of rapid decline in Arctic sea ice concentration

Sally Close, Marie-Noëlle Houssais, Christophe Herbaut

▶ **To cite this version:**

Sally Close, Marie-Noëlle Houssais, Christophe Herbaut. Regional dependence in the timing of onset of rapid decline in Arctic sea ice concentration. Journal of Geophysical Research. Oceans, 2015, 120 (12), pp.8077-8098. 10.1002/2015JC011187 . hal-01252097

HAL Id: hal-01252097

https://hal.sorbonne-universite.fr/hal-01252097

Submitted on 7 Jan 2016

HAL is a multi-disciplinary open access archive for the deposit and dissemination of scientific research documents, whether they are published or not. The documents may come from teaching and research institutions in France or abroad, or from public or private research centers.

L'archive ouverte pluridisciplinaire **HAL**, est destinée au dépôt et à la diffusion de documents scientifiques de niveau recherche, publiés ou non, émanant des établissements d'enseignement et de recherche français ou étrangers, des laboratoires publics ou privés.

AGU PUBLICATIONS

JGR

Journal of Geophysical Research: Oceans

RESEARCH ARTICLE

10.1002/2015JC011187

Special Section:
Forum for Arctic Modeling and Observing Synthesis (FAMOS): Results and Synthesis of Coordinated Experiments

Regional dependence in the timing of onset of rapid decline in Arctic sea ice concentration

S. Close[1], M.-N. Houssais[1], and C. Herbaut[1]

[1]Sorbonne Universités (UPMC, Univ Paris 06), CNRS-IRD-MNHN, LOCEAN Laboratory, Paris, France

Abstract Arctic sea ice concentration from satellite passive microwave measurements is analyzed to assess the form and timing of the onset of decline of recent ice loss, and the regional dependence of the response. The timing of the onset is estimated using an objective method, and suggests differences of up to 20 years between the various subregions. A clear distinction can be drawn between the recent onset times of the Atlantic sector (beginning in 2003) and the much earlier onset times associated with the Pacific sector, where the earliest transition to rapid loss is found in 1992. Rates of decline prior to and following the transition points are calculated, and suggest that the postonset rate of loss is greatest in the Barents Sea, and weakest in the Pacific sector. Covariability between the seasons is noted in the SIC response, both at interannual and longer time scales. For two case regions, potential mechanisms for the onset time transitions are briefly analyzed. In the Barents Sea, the onset time coincides with a redistribution of the pathways of ice circulation in the region, while along the Alaskan coast, the propagation of the regional signal can be traced in the age of the sea ice. The results presented here indicate a series of spatially self-consistent regional responses, and may be useful in understanding the primary drivers of recent sea ice loss.

Key Points:
- Maps of the timing of transition in Arctic sea ice concentration are created
- Strong regional dependence is evident in the timing of transition
- Estimates of transition time show coherency between seasons

Correspondence to:
S. Close,
sally.close@locean-ipsl.upmc.fr

Citation:
Close, S., M.-N. Houssais, and C. Herbaut (2015), Regional dependence in the timing of onset of rapid decline in Arctic sea ice concentration, *J. Geophys. Res. Oceans*, *120*, doi:10.1002/2015JC011187.

Received 29 JUL 2015
Accepted 13 NOV 2015
Accepted article online 18 NOV 2015

© 2015. American Geophysical Union. All Rights Reserved.

1. Introduction

The rapid decline in Arctic sea ice area since the beginning of the satellite era [e.g., *Serreze et al.*, 2007; *Cavalieri and Parkinson*, 2012] is perhaps the most visually dramatic change in the climate system over this period. The decrease in sea ice area has been accompanied by various other changes in sea ice properties, with a lengthening of the melt season [*Stroeve et al.*, 2014], a decrease in multiyear ice extent with concomitant thinning of the pack [e.g., *Rigor and Wallace*, 2004; *Maslanik et al.*, 2007; *Giles et al.*, 2008; *Haas et al.*, 2008] and altered ice-albedo feedback [e.g., *Perovich et al.*, 2008] being among the most important changes (more detailed discussion may be found in the recent reviews of *Perovich* [2011] and *Stroeve et al.* [2012]). This rapid decrease in sea ice coverage forms part of a broader series of Arctic-wide climate transitions, which encompass shifts in the large-scale atmospheric circulation [e.g., *Zhang et al.*, 2008; *Overland and Wang*, 2010; *Overland et al.*, 2012] with concomitant increases in surface air temperature [*Overland et al.*, 2008; *Serreze et al.*, 2009], warming of the inflowing Atlantic Water [e.g., *Polyakov et al.*, 2012; *Schauer et al.*, 2004] and an increase in freshwater storage in the Arctic Ocean, particularly within the Canada Basin [e.g., *Rabe et al.*, 2014; *Krishfield et al.*, 2014]. The climate system being coupled, it is clear that these changes in its individual cryospheric, atmospheric, and oceanic constituents do not occur in isolation. There is thus an important motivation to understand transitions in any given component of the system, such as that occurring in the sea ice, since they are likely to have both a cause and effect relationship with changes in the other components.

One of the most striking aspects of the decline in Arctic sea ice area is the nonlinear nature of recent changes in the rate of decline. It is possible that this may, in turn, be linked to the question of the reversibility of sea ice decline. Using a model-based analysis, *Lindsay and Zhang* [2005] suggest that the various exceptional forcings experienced by Arctic sea ice during the late 1980s and early 1990s may have already triggered a new regime in sea ice behavior. *Livina and Lenton* [2013] further identify a "tipping point" in 2007, finding an increase in the amplitude of the seasonal cycle of sea ice area after this time; however, these authors emphasize that this change in regime should be considered as an abrupt transition, rather than a strict bifurcation. The notion of a critical state for transition has been disputed by other authors, with *Holland et al.* [2006] finding that, in an analysis of CMIP3 models, abrupt retreat of sea ice occurred in conjunction with rapid increases in oceanic heat transport to the Arctic region, and that there was no evident

common critical state among the models analyzed in the study. Further, utilizing a 1-D model, *Eisenman and Wettlaufer* [2009] concluded that it was unlikely that sea ice loss would become an irreversible process during the transition from perennial to seasonally ice-free conditions; however, they found that such a transition may be possible under further warming, should loss of the winter ice cover occur. Prior work thus strongly emphasizes the importance of the background state, particularly of the winter sea ice, in determining summer (and indeed complete) ice loss. However, notwithstanding the evident nonlinearity in the recent sea ice tendency, our present understanding of the conditions that might signal the onset of an irreversible decline in sea ice loss remains incomplete.

The detection of the conditions that might be associated with the transition to a new regime in Arctic sea ice behavior is further complicated by the length of the observational record, which is short relative to the processes of interest: satellite records of sea ice concentration begin in 1978, and the decadal-scale length of the observational record may thus not be sufficient to describe the characteristic time scales associated with climatic variability. This issue has been addressed by a number of recent studies, using both model-based and observation-based analyses, highlighting the potentially important roles of both internal variability and low-frequency forcing in determining recent ice loss. In a study based on an analysis of models from the CMIP5 ensemble, *Swart et al*. [2015] find internal climate variability to be sufficiently large to explain recent enhanced sea ice loss. This result contrasts with the earlier analysis of *Kay et al*. [2011], who, in a study based on a single model (CCSM4), conclude that internal variability can explain only approximately half of late 20th century ice loss, and that recent changes cannot be explained solely by natural causes. Considering low-frequency influences, *Day et al*. [2012] and *Zhang* [2015] both suggest an important role of multidecadal Atlantic variability in determining Arctic sea ice extent using model-based analyses, while *Miles et al*. [2014] also find evidence of an intrinsic link between the Atlantic Multidecadal Oscillation and Arctic sea ice extent using paleoproxy records. Further to this, *Zhang* [2015] suggests that, due to this dependence on Atlantic variability, a future weakening of oceanic heat transport might lead to a hiatus in sea ice decline (consistent with the earlier work of *Holland et al*. [2006]).

Motivated by the recent shifts in the Arctic climate system noted above, some recent studies have chosen to divide the observational time series into two periods: pretransition and posttransition; for example, examining early winter sea ice variability in the Barents Sea, *Yang and Yuan* [2014] choose to divide the time period at 1997, while *Stroeve et al*. [2012], in their Figure 3, mark the division in the September total sea ice extent in 1998/1989. For studies based on statistical techniques requiring the assumption of stationarity, this division may indeed be argued to be shrewd: concomitantly with the changing mean value, decreasing SIC may be associated with either an increase or a decrease in variance at a given location, depending on the nature of the transition. Regions moving from permanent ice coverage to seasonal will experience an increase in variance, whereas those that transition from being seasonally ice-covered to completely ice-free will have an associated decrease in variance. The time series of sea ice concentration (SIC) in such regions thus violate the Gauss-Markov theorem's requirement of homoscedasticity (i.e., the trend calculated for such a series using simple linear regression will not be the best unbiased linear estimate). The question of when this division into pre/posttransition should be made is not, however, trivial. Further, the Arctic sea ice is highly seasonal both in terms of coverage and trend [e.g., *Cavalieri and Parkinson*, 2012], which raises the possibility that the timing of SIC transition may differ depending on the seasonal cycle of the region and the time of year at which it experiences the greatest response.

In this study, we address this question of possible seasonality and regional dependence, examining the timing of the onset of the recent rapid decrease in SIC in the Arctic using an objective detection method. The data used and methodology are outlined in section 2. Pan-Arctic maps of the timing of onset are presented in section 3, with a discussion of the results on a regional basis following in section 4. Some conclusions and a summary can be found in section 5.

2. Data and Methods

2.1. Data

National Snow and Ice Data Center bootstrap sea ice concentration data retrieved from the Nimbus-7 Scanning Multichannel Microwave Radiometer and Defense Meteorological Satellite Program (-F8, -F11, and -F13) and Special Sensor Microwave Imager (-F17) passive microwave measurements are used to analyze changes

in SIC (for brevity the data set will hereafter be referred to as SSMI, but comprises SMMR, SSM/I, and SSMIS data [*Comiso*, 2000, updated 2014]). The data have a spatial resolution of 25 km, and monthly data are employed in the analysis. (Analysis of a subset of daily data suggests that the results are not sensitive to this choice, and hence the monthly data set is employed to reduce the computational burden.) The data used in this study span the period 1979–2013.

For verification purposes, the analysis has been repeated using combined Advanced Microwave Scanning Radiometer—Earth Observing System (AMSR-E) and AMSR2 sea ice concentration. The data are derived using the ARTIST sea ice (ASI) algorithm, yielding a 6.25 km spatial resolution and are made available by the Integrated Climate Data Center, University of Hamburg [*Spreen et al.*, 2008]. The AMSR-E data cover the period June 2002 to September 2011, and AMSR2 span July 2012 to the present day. The availability gap between the two data sets is bridged using SSMIS data processed with the same algorithm and made available from the same source. Where the transition point is found to occur after 2002, the AMSR-based and SSMI-based analyses yield consistent estimates of behavior. We thus present only the results of the SSMI-based analysis in the following sections.

2.2. Methods

2.2.1. Processing of Data

As for many other climatic quantities, the SIC at a given location may experience strong variability on both interannual and decadal time scales. On visual inspection of such a time series, it may hence be difficult to ascertain the timing of a transition with precision, since the interplay between the varying time scales is not easy to separate. The approach that we adopt in this work is detailed further below, but may be summarized as follows: we consider the data for either a given month or season, and initially smooth the time series at each location using a LOWESS filter. We then determine whether or not a time series may be considered as a candidate for a nonlinear transition (using selection criteria outlined below). Only time series that are not classified as "stable" undergo the final stage of analysis, in which we apply the Ramer-Douglas-Peucker (RDP) algorithm [*Ramer*, 1972; *Douglas and Peucker*, 1973] to simplify the form. Using this simplified line, it is then possible to determine whether the SIC at each location has undergone a rapid transition, and, if so, at what time this decline begins. The decision is made to use the RDP algorithm here, as opposed to other previously documented methods such as change point detection, for reasons of computational efficiency: methods such as change point detection (or indeed, even optimal solution of linear piecewise regression) require a comparatively large number of operations per time series. The RDP algorithm is both considerably more efficient and also recursive, greatly reducing the run time for the analysis compared to these other methods. From a practical viewpoint, this facilitates the validation of the choice of parameters, and also makes it feasible both to apply the method to a data set of relatively high-spatial resolution and to repeat the analysis for multiple seasons.

In the first step of the analysis, the SIC time series are classified, so that locations where the SIC is considered unlikely to have undergone a transition (and hence where the algorithm will not yield a result) are not analyzed. The distribution of these classes by season is shown in Figure 1, where winter is defined as January–March, spring as April–June, summer as July–September, and autumn as October–December. First, points where no ice is present at any time during the record are classified as ice-free. Next, points that have a low mean value of SIC (less than 15%, shown in dark blue in Figure 1) are categorized. The variance at these points is too large relative to the mean state to permit accurate estimation of changes in the mean state with time, and thus the RDP algorithm does not yield meaningful results at such locations. Finally, points that are ice-free for more than 40% of the record (i.e., more than 14 years, for a record of total length 35 years for a given month/season) are classified as occasionally ice-covered. This class of time series is located at the outermost edge of the pack (shown in pink in Figure 1), and has an extremely high variance and low mean SIC. The patchy and highly variable nature of the temporal coverage makes it difficult to estimate the mean state at these locations over any given subperiod. The results that would be yielded by the RDP algorithm for such time series thus cannot be considered meaningful, since they simply highlight large-variance events. The threshold of 40% used here has been determined experimentally by evaluating the performance of the algorithm (using the root-mean-square error of the residuals from the simplified form described below) for a subset of points, selected using the ratio of the variance to the mean state. Three initial classes for which it is not possible to apply the algorithm are thus defined: ice-free, low SIC and occasionally ice-covered. All data that are not described by these classes undergo further analysis.

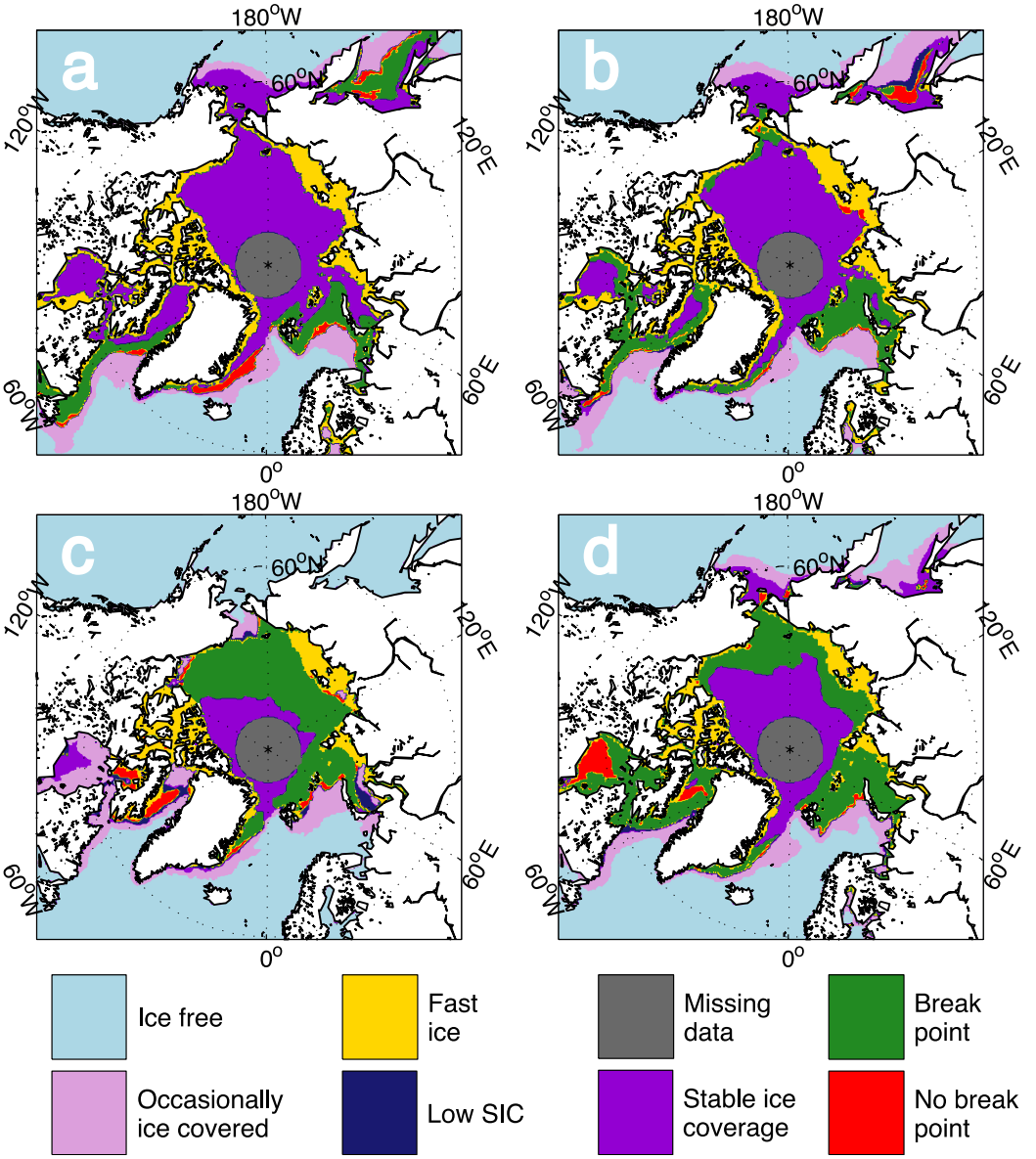

Figure 1. Map showing classification criteria for (a) winter (JFM), (b) spring (AMJ), (c) summer (JAS), and (d) autumn (OND). Regions that are ice-free (light blue), occasionally ice-covered (pink), have stable ice coverage (purple) or very weak ice coverage (dark blue) are rejected before application of the algorithm (see text for full description of categories). Grey indicates regions with missing data (not analyzed). Yellow indicates regions where fast ice is present for more than 1 year, green denotes regions where a breakpoint is detected by the algorithm, and red indicates that the algorithm fails to find a breakpoint.

For the remaining data, prior to the application of the algorithm, the presence of landfast ice must be considered. The SSMI algorithm is designed to retrieve sea ice concentration, and thus it is not certain that these data are accurate in the presence of fast ice [e.g., *Tamura et al.*, 2007]. To classify the fast ice, National Ice Center ice charts [*Fetterer and Fowler*, 2006, updated 2009] are used (full details and the processing history of these data may be found in *Fetterer* [2006]). The data are at present available only until 2007, and thus the period 1979–2007 is used here. Locations where fast ice is present for more than 40% of the time are considered to have too much "missing" data, and are not analyzed (where this threshold has again been determined experimentally). For locations where fast ice is present for less than 40% of the time, the points within the time series that are classified as fast ice are ignored by the algorithm when it is applied. This introduces additional uncertainty into the accuracy of the onset estimate, and thus all locations where fast ice is detected at any time during the study period are hatched in the presentation of our results to indicate

that the analysis should be treated with caution here. Nevertheless, the results found for the locations containing some fast ice show spatial homogeneity with the adjoining regions where no fast ice is found, suggesting that there is some value in the information provided by the analysis here. Finally, since data covering this period are not yet available, it is not possible to account for the presence of fast ice during the final 6 years of the study period (2008–2013). However, since the Arctic fast ice coverage has been in decline since the early 1990s [*Yu et al*., 2014], it is considered unlikely that fast ice will have been present during these most recent years in regions outside those where fast ice has already been detected earlier in the period. Locations where fast ice is present are marked in Figure 1 for information. (Any location in which fast ice is detected in more than 1 year is classified as being partially fast ice-covered.)

The processing of the data is, by necessity, a point-wise operation, and the following procedure thus describes the analysis applied to the time series of SIC at each location. The initial filtering of the data is performed for monthly/seasonal data, using a simple LOWESS filter [*Cleveland*, 1979] with a 5% span. (The LOWESS filter is a nonparametric fitting method that applies locally weighted least squares fitting, with the data being weighted using the tricube weight function to assign larger weights to data lying nearer to each given point of the time series and smaller weights to those lying further from each point, and the span defining the amount of data used in each local fit.) This filtering reduces any extremes associated with interannual variability, and thus avoids the introduction of extraneous complexity when the RDP algorithm is applied, since our primary interest here is in describing the long-term change. It is, however, necessary that the span value should be relatively small to ensure that the shape of the time series is not strongly deformed, so that the transition point is detected with a reasonable precision. The value of 5% was thus determined prior to the analysis by testing of a number of profiles, spanning a range of behaviors. Following this step, we calculate the linear trend over the full time series (again for each month/season), and the change in mean SIC between the first and last 5 years of the time series. (The use of two estimates of long-term change here is a precaution against the possibility of misfit induced by interannual variability in the linear trend estimation.) Time series having an equivalent change of less than 10% in SIC over the full period in both estimates are considered unlikely to have undergone a transition, and are classified as stable (shown in purple in Figure 1; this value also corresponds to the tolerance used in the application of the RDP algorithm below). Having extracted the time series that are considered unlikely to have undergone a transition, the form of the remaining time series is then simplified by application of the RDP algorithm.

2.2.2. RDP Algorithm Description

The RDP algorithm is widely applied in polyline simplification applications (a geophysical example being in the production of the Global Self-consistent, Hierarchical, High-resolution Shoreline Database [*Wessel and Smith*, 1996]), and functions by reducing the number of vertices of a given input according to a specified tolerance, ϵ. Figure 2 illustrates the application of the algorithm to a sample time series. Beginning with the straight line joining the beginning and end points (shown by the blue dashed line in Figure 2a), the orthogonal distance between this line and each point comprising the input is calculated (Figure 2a, inset). If the orthogonal distance between the line and the vertex lying furthest from this line is greater than ϵ, the line is split at this point, and the procedure recursively applied to the two resulting pieces (Figure 2b; note that at each recursion, the orthogonal distance is recalculated relative to the new segments of the line that result from the split at the previous recursion). If the distance is less than or equal to ϵ, no further splitting occurs, and the simplification process is considered to be completed (Figure 2c shows an example in which the simplified form is achieved after three recursions). After analysis of the linear trends and the standard deviation associated with the data, a tolerance of $\epsilon = 10$ (/% SIC) was decided to be appropriate, and the functioning of the algorithm using this value verified using a subset of data showing varying behaviors (both for partially covered to ice-free and permanent to partially covered transitions, and also for time series that do not exhibit nonlinear behavior). The verification is performed by local minimization of the RMSE, subject to the constraint that the breakpoint is stable as a function of ϵ. Visual inspection of the subset of time series and calculated onset times was then performed as a final sanity check.

In the final step of the analysis, the gradients associated with the simplified time series are evaluated. We split the time series at the vertex after which the greatest decline in SIC occurs, and calculate the linear trend associated with the data prior to and after this point (hereafter referred to as the breakpoint or onset time). For regions that transition to an ice-free state, the time series is truncated to include only the part of the time series where the LOWESS-filtered SIC is greater than 5%, to ensure that the rate of decrease is

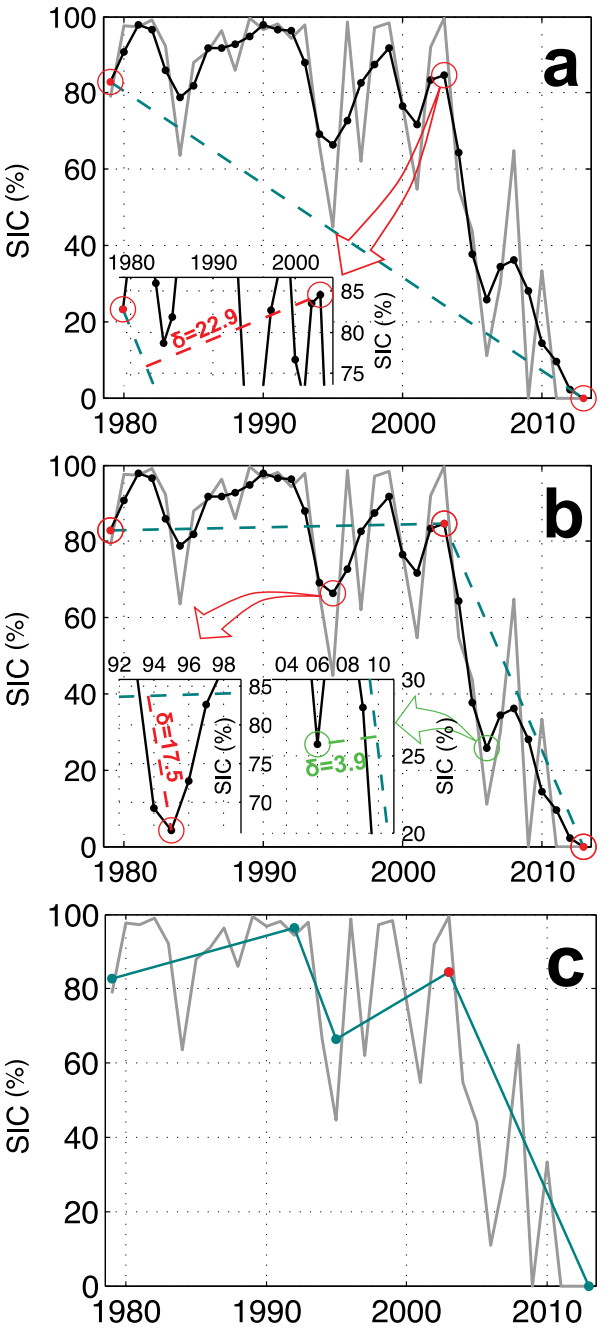

Figure 2. Illustration of the application of the Ramer-Douglas-Peucker algorithm to a sample time series selected from the Barents Sea in July. (a) The first application of the algorithm to the input time series, (b) the second recursive call, and (c) the final, simplified time series. For all figures, the grey line shows the raw, unsmoothed time series. The black line shows the LOWESS-filtered data, with the input points being marked by black dots. In Figure 2a, the circled dots highlight the two end points used to define the reference line (dashed blue line). The black point surrounded by a red circle is the vertex lying furthest from this line. The inset shows the orthogonal distance, δ from the point to the line. Here $\delta > \epsilon$ and will lead to a recursive call ($\epsilon = 10$ in this study). In Figure 2b, the two insets show the orthogonal distances between the two newly defined lines and their most distant vertices. The left inset (arrow and point circled in red) again has $\delta > \epsilon$ and will result in a further recursive call. In the right inset (green arrow/circled point), $\delta < \epsilon$: this vertex will not exist in the simplified time series, and the simplification procedure terminates for this segment. In Figure 2c, the blue line shows the final simplified time series; the breakpoint is marked by a red dot.

calculated only over the part of the time series where SIC is present and declining. Two *t* tests are then used to determine first whether or not the change in gradient of the latter part of the time series is significant relative to that of the first part, and, second, whether or not the two parts of the time series have different means. Time series where no significant change is found in either test are classified as "no breakpoint" (shown in red in Figure 1). For time series where a breakpoint is found (shown in green in Figure 1), a final approximation of the onset time is obtained. Based on the sensitivity to the initial LOWESS filtering and response to the choice of ϵ, the resulting breakpoints are estimated to have an associated error of approximately ± 3 years, both for the seasonal and the monthly analyses. (Note that for regions containing fast ice, the expected uncertainty on the estimate is not quantified.) For brevity, and because the results are compatible with those of the seasonal mean analysis (which may, furthermore, be considered to be a more stable estimate), maps for individual months will not be shown in the following sections. Results obtained from the analysis of 3 month means of the data are hence presented, yielding seasonal values for the transition times (where the seasons are defined as previously).

2.2.3. The Form of the Ice Loss Behavior

Previous work from the literature suggests that sudden ice loss may be manifest not only as a sudden increase in the rate of decline, but also as a step-change behavior [e.g., *Livina and Lenton*, 2013]. In an attempt to further classify the evolution of the SIC by region, the extent to which various types of behavior describe the SIC time series at each location has been evaluated. Using the breakpoints detected previously, three models have thus been fitted to the raw SIC seasonal time series, representing: (i) a step-function (linking two periods of zero trend, but different means), (ii) a linear decrease throughout the time series, and (iii) two distinct periods of linear change, with one gradient for the period before the onset time obtained from the algorithm, and a second gradient for the period after (the two fits are

constrained to have the same value of SIC at the onset time, so that the resulting time series of predicted values is continuous). The root-mean-square error (RMSE) for each model is compared, allowing the most appropriate fit for each region to be determined. In all seasons and all regions, model (iii), representing a transition between two linear trends, is found to be significant at the 5% level and to yield the lowest RMSE, confirming that the use of a breakpoint model provides a valid approximation of the SIC system.

3. Pan-Arctic Results

The classification of the ice into various categories, shown in Figure 1, highlights that the only regions where breakpoints are found in all seasons are the Barents and western Kara Seas. In spring and winter, breakpoints are also identified along the eastern coast of Greenland, in Baffin and Hudson Bays, and in the Labrador Sea. However, on the whole, the Arctic-wide coverage in winter and spring is broadly classified as "stable" (total change in SIC $<$10%). The classification in summer and autumn contrasts strongly with the winter and spring, with the stable ice area being greatly reduced (especially in summer). Of the area where ice coverage is greater than 15% (and no fast ice is present), the regions where a breakpoint is found (Figure 1) comprise 70% of this total area in summer and 51% in autumn, compared to 26% in spring and 23% in winter (the area occupied by the class defined as stable ice is thus 30% in summer, 49% in autumn, 74% in spring, and 77% in winter). Regions where it is not possible to find a breakpoint because the variability is too strong are generally located either near to the edge of the pack or at the limit of the fast ice extent (shown in red in Figure 1).

The pan-Arctic maps of onset time of rapid decline produced from the application of the algorithm are shown in Figure 3 for both summer and autumn. Winter and spring are not shown, since, as noted above, breakpoints are found only in localized regions (cf. Figure 1) and these regional breakpoints are consistent with those shown for the same areas in summer and autumn, with onset times of ca. 2004 in the Barents and Okhotsk Seas, and in the early 1990s ($\sim$1992–1995) in the Hudson and Baffin Bays and the Labrador Sea. The maps of onset time suggest that Arctic sea ice variability is strongly determined by regional influences. We begin here by summarizing the broad-scale patterns; a more detailed discussion of regional features will then follow in the next section.

Perhaps the largest-scale contrast evident in Figures 3a and 3b is that between the relatively recent onset time detected in the Atlantic sector ($\sim$0–120°E) and the earlier onset times noted in the Pacific sector. This difference is particularly evident in the summer between the early onset times found in the East Siberian Sea and Beaufort Sea in the Pacific sector ($\sim$1992–1996), and the much more recent onset time that characterizes the Barents and Kara Seas, where much of the region transitions in 2003/2004.

In summer, the regional maps broadly suggest that the transition regions may be separated into two bands: one with strong spatial dependence, spanning the exterior ice edge, and an interior band where the onset year is later, and much more uniform across the Arctic. A slight difference is nonetheless noted in the interior band between the Eurasian Basin and the region lying to the east of the Lomonosov Ridge. In the Eurasian Basin, this band has an onset year ca. 2009 and a spatial pattern that hints at a link to the bathymetry, and contrasts with the wide, extremely uniform region having onset year ca. 2005 that comprises the rest of the interior band. Generally, the onset year increases northward, consistent with the ongoing retreat of the sea ice edge associated with recent reductions in sea ice area [*Parkinson and Cavalieri*, 2008]. Despite the strong longitudinal dependency, regions of uniform onset tend to have zonal extents that are much larger than their meridional extents.

The band spanning the interior of the pack in summer, having an onset time later than 2005, is largely absent in autumn. Nevertheless, relics of this band can still be identified in autumn along the Nansen Basin slope and near the Chukchi Plateau. Arguably the strongest contrast between the summer and autumn is the presence of the two bands of early transition year in summer (ca. 1992/1995, shown in pink/blue in Figure 3a) extending northward away from the eastern Siberian coast/Bering Sea region. A remnant of this pattern is still present adjacent to the Alaskan coast in the autumn analysis; however, on the whole, the Pacific sector of the Arctic is dominated in autumn by a uniform pattern of transition year in ca. 2001/2002 (shown in green/yellow in Figure 3b). This timing is similar to that found in the region spanning the inner basins of the Laptev and East Siberian Seas and along the coast of Alaska in summer. Despite the earlier onset times evident in the Pacific sector of the Arctic Ocean in summer, certain features of the summer and autumn maps of onset time

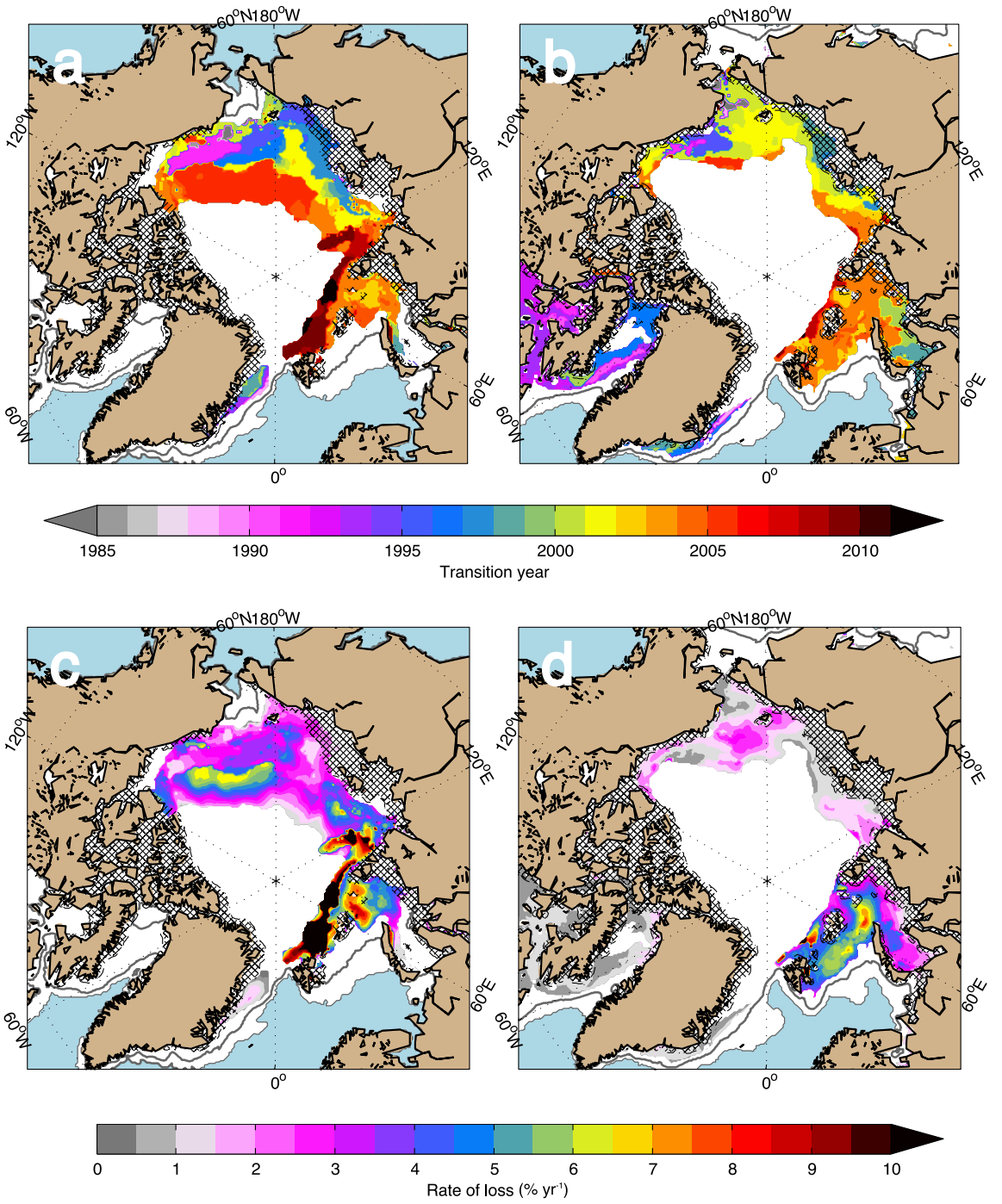

Figure 3. (a) Summer and (b) autumn maps of time of onset of rapid decline. (c) Summer and (d) autumn rates of loss after the onset times shown in Figures 3a and 3b. Hatched areas indicate the presence of fast ice, which may cause inaccurate estimation of the onset time. Blue regions are completely ice-free, while the grey line indicates the partial ice coverage threshold (40% of years have SIC > 0) applied in this study. White indicates that no breakpoint was found at a given location.

are thus rather comparable. Where different onset times are found between the summer and autumn, with the exception of a small area of the Kara Sea, the autumn onset time is later than that of the summer.

To further investigate the large-scale patterns of transition, the rates of change in SIC before and after the transition times detected above are considered for summer and autumn. Prior to the onset of rapid loss, the rates of loss show no spatial dependency (not shown), and the mean rate of loss for both seasons is

Table 1. Summary of Summer Regional Analysis[a]

Region (Figure Reference)	Variance Before (%) Mean	(Range)	Variance After (%) Mean	(Range)	Mean State Before (%) Mean	(Range)	Mean State After (%) Mean	(Range)
Barents Sea (Figure 6a)	679	(677–748)	310	(163–670)	59	(60–55)	21	(16–26)
Nansen Basin slope (Figure 6b)	52	(48–252)	560	(523–N/A[b])	86	(84–86)	62	(52–70)
Off-shelf East Siberian Sea (Figure 8a)	5	(5–117)	517	(437–517)	96	(95–97)	80	(79–83)
East Siberian Sea (Figure 8b)	479	(479–537)	655	(633–710)	83	(83–83)	62	(57–65)
Off-shelf Alaskan coast/Canada Basin (Figure 9a)	189	(189–221)	621	(621–650)	91	(90–91)	67	(62–72)
Alaskan coast (Figure 9b)	198	(146–282)	591	(495–703)	85	(84–86)	52	(47–56)

Region (Figure Reference)	Onset Time	Postonset Rate of Loss (%/yr) Mean	Range
Barents Sea (Figure 6a)	2004	5.5	4.0–7.7
Nansen Basin slope (Figure 6b)	2008–2010	12.8	4.6–N/A[b]
Off-shelf East Siberian Sea (Figure 8a)	2004–2005	2.7	2.0–3.4
East Siberian Sea (Figure 8b)	1996–2001	2.8	2.2–3.4
Off-shelf Alaskan coast/Canada Basin (Figure 9a)	2005	3.0	2.4–3.9
Alaskan coast (Figure 9b)	1992/1995	3.3	2.8–3.9

[a]The variance, mean state, and postonset rate of loss obtained by taking the calculated onset time are indicated by the "mean" columns for these respective estimates, while the ranges are obtained by repeating the calculations with the onset time (and associated onset value of SIC) shifted by ±3 years, corresponding to the maximum uncertainty range.
[b]The onset year is too close to the end of the study period to permit calculation of the upper bounds for this region.

0.4%/yr (not significant). However, after the onset of rapid loss, coherent spatial and temporal structure can be found. Figures 3c and 3d show the rate of loss after transition for summer and autumn. The strongest rates of loss are found in the Barents Sea and along the Nansen Basin slope, and the rates of loss are stronger in summer than autumn. Generally, as for the maps of onset time shown in Figures 3a and 3b, there is thus a large-scale contrast between the rates of loss in the Atlantic and Pacific sectors, with earlier onset times generally corresponding to a slower posttransition decline.

The error in the estimate of postonset rate of decline associated with the 3 year uncertainty in onset time is detailed in Table 1 for the various regions that will be explored in section 4. The uncertainty is greatest at the Nansen Basin slope, where the onset time is recent, the onset state (i.e., SIC at time of onset) high and the rate of decline very rapid. The lowest uncertainty is associated with the region where the onset year is early (ca. 1992/1995 lying along the Alaskan coast), and the form of the decline rather linear. Were the trends at onset time to be extrapolated forward, the combined uncertainties from the onset times and rates of decline after transition would imply a mean uncertainty in the time required to reach an ice-free state of 7 years for summer and 10 years for autumn. However, given that the regions for which we calculate the postonset rate of decline have already experienced a statistically significant discontinuity in either the mean state or the rate of decline, there is no a priori reason to suppose that a linear model will hold between the time of onset and the time at which these regions become ice-free.

The change in variance between the preonset and postonset periods, and the mean state after onset are shown in Figures 4a–4d for summer and autumn. It is clear that in both summer (Figure 4a) and autumn (Figure 4b), there is a widespread tendency for the variance to increase after the transition. The increase is generally weaker in autumn compared to summer, consistent with the more stable ice coverage and weaker trends (not shown, e.g., cf. *Cavalieri and Parkinson* [2012]) during the autumn.

Figures 4c and 4d show that the mean state remains relatively high after the onset time over much of the inner part of the region where breakpoints are found. To clarify the states of the SIC before and after the transition, we further classify the time series at each location according to the type of transition. We follow the marginal ice zone definitions used by *Strong and Rigor* [2013], and considering the mean states prior to

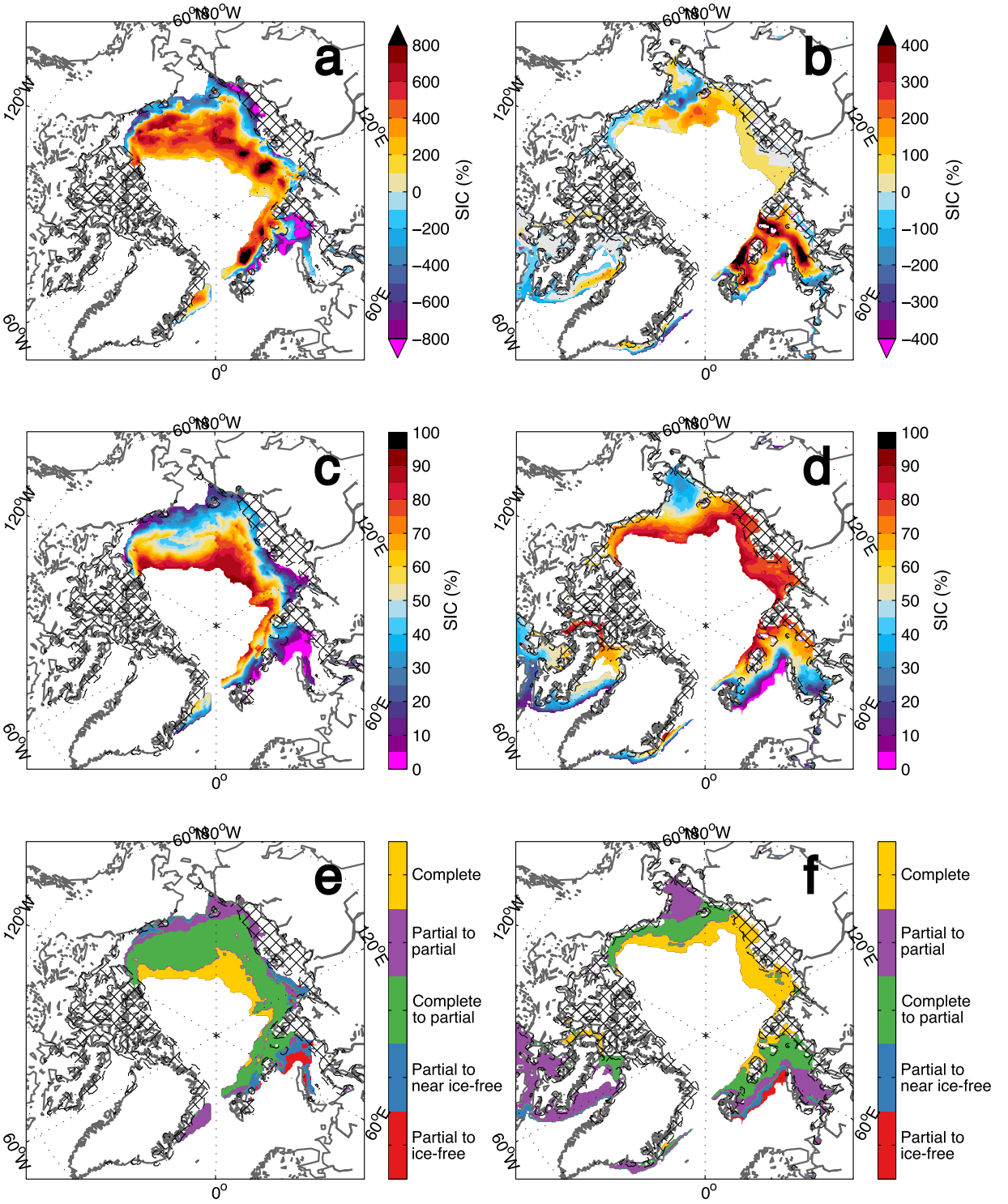

Figure 4. Change in variance after the onset time for (a) summer, (b) autumn (where positive signs represent an increase in variance after transition). Mean SIC after onset for (c) summer, (d) autumn. Classification of transitions for (e) summer, (f) autumn.

and after the transition, the descriptor "complete" is assigned where the SIC is $\geq 80\%$, "partial" to $15\% < \text{SIC} < 80\%$, "near ice-free" to $0 < \text{SIC} \leq 15\%$ and "ice-free" is assigned to states where the median SIC is 0% (since the transition to ice-free conditions is never instantaneous, and therefore the mean after onset is never zero as it always includes at least 1 year in which the ice is present, but declining, while

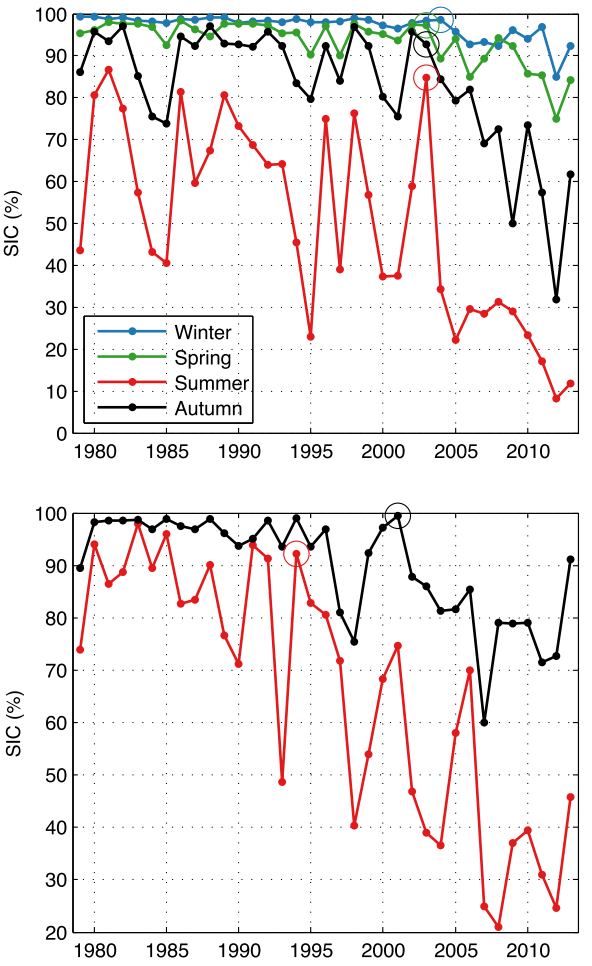

Figure 5. (top) Seasonal time series for the Barents/Kara Sea (average over region a of Figure 6). (bottom) Summer and autumn time series for Alaskan coast (average over region b of Figure 9). The breakpoints found by the algorithm for each time series are circled. The regions used here define areas where breakpoints are present in all of the seasons shown in each plot.

transitioning to the new state). The classification of the type of transition for the various breakpoint regions is then shown in Figures 4e and 4f for summer and autumn, respectively.

The significance of the changes in variance shown in Figures 4a and 4b is evaluated using the Breusch-Pagan-Koenker test (to test for the presence of heteroscedasticity over the full length of the time series) and the Brown-Forsythe test (to test the significance of the differences in variance between the preonset and postonset periods). In the general case of the Breusch-Pagan-Koenker test, this indicates that the variance differs significantly within the time series and, more specifically, the Brown-Forsythe test indicates that the variance is significantly different before and after onset (both tests are performed at the 95% significance level). The two tests yield geographically co-located positive results, with significant changes in variance over the entire complete and complete-to-partial transition regions in both summer and autumn, and also the partial-to-partial transition regions in the Barents Sea and Hudson/Baffin Bays in autumn.

From Figures 4e and 4f, it can be seen that in summer the dominant class of transition is from complete to partial ice coverage, while in autumn the behavior is more mixed. Consistently with the results of *Strong and Rigor* [2013], very few regions transition to an ice-free or near ice-free state, so that the increase in the area of the regions categorized as partially covered corresponds to a northward expansion of the marginal ice zone, with little associated change in the position of the southern ice edge. There is a strong similarity between plots a and e, and b and f of Figure 4, corresponding to the notion that time series that have near-complete SIC exhibit only weak interannual variability, whereas partially covered regions show much greater interannual variability. Regions that transition from partial ice coverage to ice-free or near ice-free similarly have a reduction in variance, where the weaker (or lack of) ice coverage is associated with weaker (or zero) variance. Transitions between two partially covered states may be associated with either an increase (as in the Kara Sea in autumn, cf. Figures 4b and 4f) or a decrease (as along the coast of Alaska in summer, cf. 4a and 4e) in variance. Recalling the proportions of ice-covered area that the breakpoint regions comprise, this therefore suggests that, of the ice-containing area of the Arctic, in summer [autumn] approximately 48% [33%] can be classified as only partially covered, 10% [3%] transitions to being ice-free or nearly ice-free, and 12% [14%] remains in the "complete" (i.e., SIC $>$ 80%) category after the transition.

Considered in conjunction with the uniform response in the Barents Sea throughout the year, the coherence between seasons noted previously (Figures 3a and 3b) suggests the presence of large-scale regions where the onset time is independent of the season. While our analysis focuses primarily on summer and autumn, since these are the seasons over which the widest coverage of breakpoints is found, here we

consider the links between the various seasons. Figure 5 shows time series of all seasons for the Barents/Kara Sea area mean (the only regions where breakpoints are found in all seasons), and of summer and autumn for the early onset region lying along the Alaskan coastline, where the transition year occurs between 1992 and 1996 in summer.

In the Barents Sea, breakpoints are found in approximately 2004 in all seasons; this consistency in the timing of onset hints at coherent behavior between the seasons, motivating the further examination of their form and correlation. The top plot of Figure 5 highlights that the greatest changes do indeed occur after the 2003/2004 breakpoint in all seasons in this region, with the strongest decline in summer and autumn, and a weaker response in spring and winter. To further explore the coherency between the seasons, the piecewise trend is removed from the time series (i.e., separate trends are removed for the period 1979–2003 and 2004–2013), and the anomaly around the trend calculated. The correlation between these anomaly time series is then examined. With the exception of either the following or preceding winter with summer, and any season with the following winter, all correlations between seasons (calculated between the preceding and following winter for a given year only) are significant at the 95% level. The strongest correlation occurs between summer and autumn ($r = 0.64$). However, for all seasons except spring, there is a statistically significant change in variance after the onset time (increasing for winter and autumn and decreasing for summer), which may dominate the correlation. The calculation is thus repeated with the two parts of the time series being normalized separately before and after the onset time to verify that the correlations are not artificially inflated by this effect. This is found not to be the case: all correlations remain significant (with some combinations of seasons having an increase in correlation and some a decrease). This thus suggests that, for the sole region where breakpoints are found throughout the year, there is coherency between the seasons not only in the timing of the transition (supported by the breakpoint analysis) but also at the interannual time scale (supported by the correlation analysis). Even if the rates of decline after onset are different and seasonally dependent, the significant correlations between the seasons found here suggest that the coincident timing of onset may be related to their covariability.

The analysis of the link between seasons in the Barents and Kara Seas is of interest because of the presence of breakpoints in all seasons. However, this also raises the possibility that it is a unique case, and that the link between summer and autumn might be different in other regions. An example of another region where breakpoints are found in both summer and autumn is thus shown in the bottom plot of Figure 5 for the region lying off the Alaskan coast where a relatively early onset year of 1992/1995 is found in summer, but a later value of 2001 found in the autumn. (Note that the time series shown in the bottom plot of Figure 5 is a mean over the region, thus the onset time is modified.) For the sake of brevity, time series are not shown for all regions where breakpoints are found in both seasons, since the general relationship between the time series can be characterized using the forms shown here. In these regions, the SIC in autumn generally has a higher mean state at the beginning of the time series than that of the SIC in summer. The summer time series is further characterized by stronger interannual variability from the beginning. This interannual variability is nevertheless significantly correlated between the two seasons: for the time series shown here, $r = 0.63$ for the piecewise anomaly time series (remaining approximately constant at $r = 0.64$ after normalization of variance by period). We thus hypothesize that the difference in onset time between summer and autumn here relates to the ability of the ice to recover from a forcing which is coherent throughout these seasons, but would lead to the summer ice cover failing before that of the autumn.

In the following section, the regional responses will be considered in greater detail. Given both the numerous similarities in the maps of onset time between summer and autumn noted above, and also that the regional onset times for winter and spring (not shown) are consistent with those found in summer and autumn, only maps and time series from the summer will be presented. However, where differences exist between the seasonal results (e.g., in the East Siberian Sea), these will be discussed below. For ease of reference, a summary of this regional discussion is provided in Table 1.

4. Regional Discussion

4.1. Barents and Kara Seas and Nansen Basin Slope

In all seasons, the maps of onset time in the Barents and Kara Seas demonstrate strong spatial uniformity, having a transition time approximately in 2003/2004 (Figure 6). This transition takes the form of a sudden decrease in both the variability and mean state of the SIC relative to the period 1979–2003 (Figure 6a), and

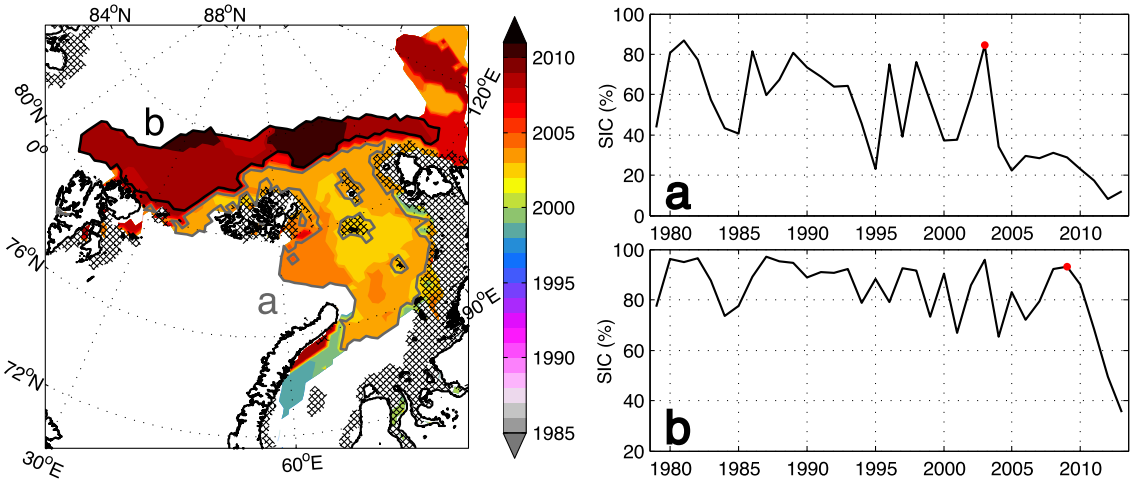

Figure 6. Map of summer transition times for Barents and Kara Seas and the Nansen Basin slope. Hatching indicates the presence of fast ice. Area mean time series are shown in Figures 6a and 6b for the two regions labeled on the map (comprising areas where the onset year is between 2002 and 2005 and after 2008, respectively). Red points indicate the area mean breakpoints. Area a is outlined in grey, and area b in black on the map.

the persistence of this form and consistent onset time throughout the seasons (Figure 5, top) is suggestive of a low-frequency forcing, that may implicate a persistent change in atmospheric forcing, an oceanic role, or an effect related to sea ice memory, either through persistence or reemergence.

In their analysis of regional changes in Arctic SIC, *Cavalieri and Parkinson* [2012] note that the Kara and Barents Sea show an increase in magnitude of trend between their analyses covering the period 1979–2006 and 1979–2010, suggesting an accelerated loss rate in the 2006–2010 period that is consistent with the 2003/2004 transition points found here. A variety of processes have been conjectured to influence the sea ice extent in the Barents Sea. In the atmosphere, these include both large-scale [*Deser and Teng*, 2008] and also localized forcing at interannual [e.g., *Koenigk et al*., 2009] to decadal [e.g., *Kwok*, 2009] timescales. However, numerous studies have also posited an important role of oceanic forcing in this region, either through the local generation of heat anomalies [*Schlichtholz*, 2011] or by their advection into the region via the warm, inflowing Atlantic Water (AW) [*Årthun et al*., 2012; *Sandø et al*., 2014]. The transition time occurring in 2003/2004 found here would be consistent with the findings of *Skagseth et al*. [2008], who note a maximum in AW heat flux through the Barents Sea Opening during these years (their Figure 2.6); however, a robust link to the 2004 ice cover decline in the Barents Sea has not been proven [*Herbaut et al*., 2015]. Given that the recent warming of AW is one episode in a series of such events that are reported to have begun earlier (in the 1990s, e.g., *Quadfasel et al*. [1991]), another forcing mechanism may also be implicated in this transition.

To investigate the viability of potential forcing mechanisms associated with the onset times found here, atmospheric fields from the ERA interim reanalysis [*Dee et al*., 2011] are analyzed alongside ocean data from the EN4 objective analyses [*Good et al*., 2013]. In addition to observations drawn from the World Ocean Database (WOD) [*Boyer et al*., 2013], the EN4 analysis also includes data compiled within the scope of the Arctic Synoptic Basin Wide Oceanography project, drawing on several sources not presently included in the WOD, with the aim of improving data coverage in the Arctic region. The grid has 1° horizontal resolution and 42 vertical levels, and an uncertainty estimate for each grid point is supplied with the analysis (full details can be found in *Good et al*. [2013]), which is taken into account in our analysis. Using these data, the heat content of the upper 100 m of the ocean (top 10 vertical levels of the gridded data) at each grid point is calculated over the Barents Sea region, and analyzed to check for statistically significant changes in the mean state using the regime shift detection method of *Rodionov* [2004]. A transition is found to occur ca. 1998 across the region, agreeing with previous work in the literature [e.g., *Karcher et al*., 2003]; however, no shift is detected either during 2004 or the years that immediately precede it, suggesting that, for the 2004 transition, changes in the ocean do not precede those in the ice.

The SLP gradient index defined by *Herbaut et al*. [2015] as the difference between SLP over Svalbard and Novaya Zemlaya, and found therein to strongly influence winter ice cover in the north of the Barents Sea, is also examined. The index is derived from the December–February mean SLP. Again using the regime shift

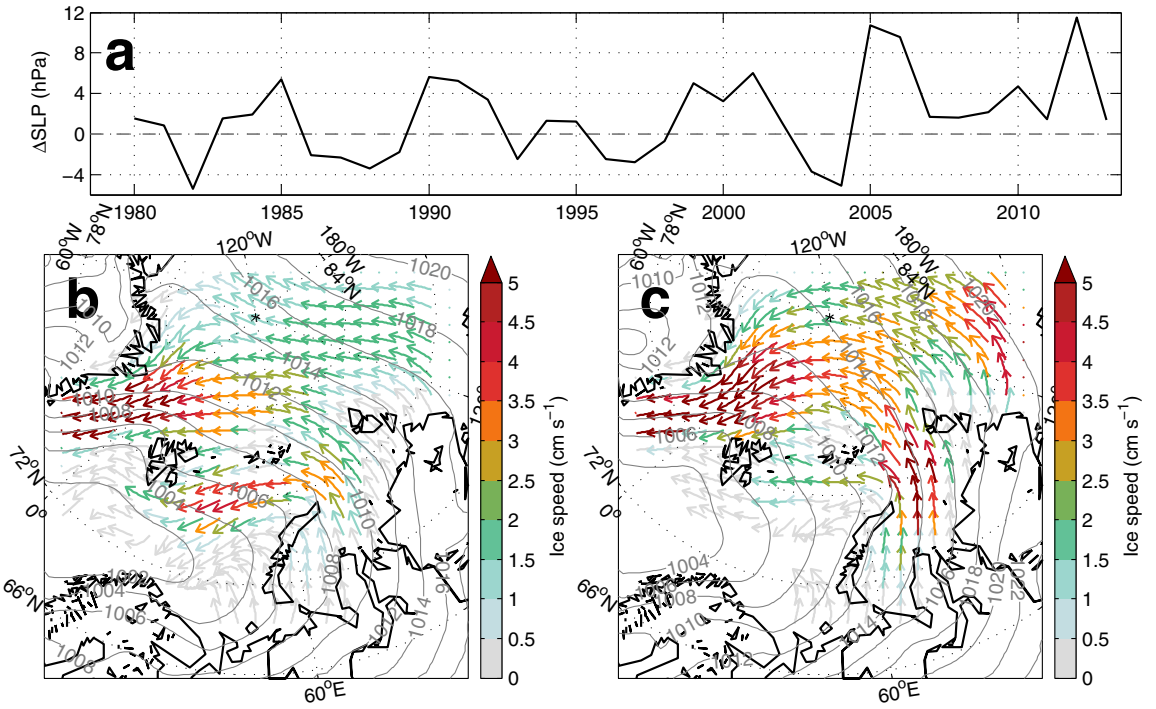

Figure 7. (a) DJF SLP difference between Svalbard and Novaya Zemlaya. DJF ice motion mean state averaged over (b) 1980–2004, (c) 2005–2012 overlaid with mean contours of SLP.

method of *Rodionov* [2004], the index is found to undergo a statistically significant step change between 2004 and 2005 (Figure 7a), oscillating between positive and negative values prior to this time, but remaining persistently positive afterward. This change reflects a shift in the orientation of the isobars, which have a more meridional alignment and also extend further northward in the 2005–2012 mean than that of 1980–2004 (Figures 7b and 7c). Associated changes are observed in the ice motion (analyzed using Polar Pathfinder 25km sea ice motion vectors, available over the period 1978–2013 [*Fowler et al.*, 2013], and again shown in Figures 7b and 7c), with the distribution of export from the Kara Sea changing from a relatively zonal configuration, leading to a direct ice import into the Barents Sea, to a more meridional orientation, which favors instead an import into the Arctic Ocean. This change in configuration is rather similar to the two extreme cases shown in *Kwok et al.* [2005, Figure 2], with the post-2004 mean shown here exhibiting similar flow patterns to that found to be associated with ice flow from the Barents Sea into the Arctic Ocean in 1999–2000 in that work.

A change in configuration can also be noted in the circulation of ice exported to/imported from the Arctic Ocean to the Barents Sea through the region between Svalbard and Franz Josef Land, with the second period hinting at a tendency to favor export from the Barents Sea into the Arctic Ocean, rather than import from the Arctic Ocean into the Barents Sea (Figures 7b and 7c). While the ice velocities in this region are notably smaller than those of the ice originating in the Kara Sea ($\sim$1 cm s^{-1} cf. $\sim$5 cm s^{-1}), it should be borne in mind that relatively weak velocities may nevertheless translate into considerable changes in volume transport. However, lacking adequate data, it is not possible to calculate changes in this quantity.

While their results only cover the period up until 2007, the previous estimates made by *Kwok* [2009] of the ice area fluxes through the gateways between Franz Josef Land and Severnaya Zemlaya, and between Svalbard and Franz Josef Land provide further support to the idea of a redistribution outlined above. Their results demonstrate an increased outflow into the Arctic Ocean through the Franz-Josef Land-Severnaya Zemlaya gateway after 2004. Further, their analysis shows that the magnitude of the ice flow through the Svalbard-Franz Josef Land gate is close to zero after this time. In combination, these results suggest that changes in atmospheric forcing ca. 2004 could plausibly have effected changes in the 2005–2012 mean ice circulation of this region, with an enhanced ice export from the Kara Sea after this time that passes into the Arctic Ocean, rather than into the Barents Sea as in the earlier period, and that is not returned to the Barents Sea through the Svalbard-Franz Josef Land gate. The timing of this redistribution is compatible with the onset time derived here for the Barents Sea.

To the north of the Barents and Kara Seas, along the slope of the Nansen Basin, a coherent region is found where the onset time is later than in the surrounding regions. The most recent onset of rapid ice loss found in this study occurs here, in summer, with transitions occurring between 2007 and 2010 (Figure 6). The time series for this region show a stable, high ice coverage until the transition point, following which rapid loss to partially covered conditions occurs (Figure 6b). While the distribution of onset time within this region varies over a 4 year period (2008–2011), the form of the loss is the same throughout. The ice loss here is extremely rapid, with a monotonic decline that represents a loss of $>$50% of the sea ice cover in less than 5 years (cf. Figure 3c).

The alignment of the band of late onset time with the bathymetry of the slope hints that an oceanic influence may be implicated in the transition. In support of this notion, the spreading of the warming AW signal along the continental margins has been reported by several studies [*Schauer et al*., 2004; *Dmitrenko et al*., 2008]. Further, it has been suggested that upward transport of heat from the warming subsurface Fram Strait AW branch could play a role in controlling ice loss [*Polyakov et al*., 2010, 2011a, 2011b]. It is noted in these studies that this mechanism would be particularly applicable under weakening stratification, such as that suggested by recent changes in the Eurasian Basin, where salinification of the surface layer associated with a changing balance between the freshwater content distribution of the Canada and Eurasian Basins [*Morison et al*., 2012] in conjunction with the warming of the inflowing AW would combine to create these conditions.

Previous work by *Alexeev et al*. [2013] presents an observation-based analysis of AW temperature in the Fram Strait region, and relates this to the thinning of the overlying sea ice between Fram Strait and Severnaya Zemlya. It is noted in their study that field campaigns have shown the AW to be in direct contact with the sea ice in the autumn of 2004, 2006, and 2008; the corresponding time series shows the AW temperature to be consistently warmer than the 1960–2011 mean after 1998, with 2006 and 2011 being the warmest and second warmest years (their Figure 1). The timing suggested therein is thus very similar to that found in our study, where we find transition points in 2008 in the northern Barents Sea adjacent to the Nansen Basin slope in spring, and after 2009 over a wide region along the slope in summer. A relationship between AW and sea ice thickness has also previously been reported upstream, adjacent to Svalbard, by *Tverberg et al*. [2014], and between AW and SIC in the same locality by *Onarheim et al*. [2014]. It is possible that the minimum reached in the final years of the time series may also be related to the exceptional minimum of Arctic sea ice that occurred in 2012, and which was particularly marked in the Atlantic sector, with exceptional sea ice retreat to the north of the Barents Sea. This event has been ascribed to the passage of an intense cyclone [*Simmonds and Rudeva*, 2012], in combination with prolonged prior thinning of the pack ice [*Parkinson and Comiso*, 2013; *Zhang et al*., 2013]. While the transition points noted here occur in advance of this event, the sudden decrease in SIC in the later part of the time series may bear its signature.

4.2. Laptev and East Siberian Seas

Transition points are found in the Laptev and East Siberian Seas in summer and autumn. As before, a map of summer transition times and associated sample time series are shown in Figure 8.

In summer, in the northwestern corner of the region shown in Figure 8, a continuation may be found of the band having an onset time in approximately 2009 that was noted along the slope of the Nansen Basin in Figure 6. On approaching the Laptev Sea, this band appears to curve northward, approximately along the 120°E meridian. The mean time series of this patch (not shown) exhibits a similar form of decline to that shown in Figure 6b, with a sudden decline in SIC following a previously stable period where variability is negligible.

Figure 8 shows a banded structure in the onset times (blue-yellow-orange) extending northward across the region between approximately 130–180°E. Here the onset year increases between 1992 near to the coast to $\sim$2001 in the central band, which in turn adjoins a region where the onset year is 2005 (again, with the onset year increasing northward as the ice edge retreats). The band corresponding to a transition in 2005, found in summer between ca. 140–180°E, 78–82°N (Figure 8a) represents a region that passes from having almost complete ice coverage at the beginning of the time series to partial ice coverage, characterized by increased interannual variability, over the final decade of the study period (Figure 4a and 4e). This region adjoins an area with the same onset time lying to the north of the Chukchi Sea/Alaskan coast, and the time series for both regions have a similar form (cf. Figure 9a). Remnants of this region persist into autumn (not shown; the time series again has a similar form).

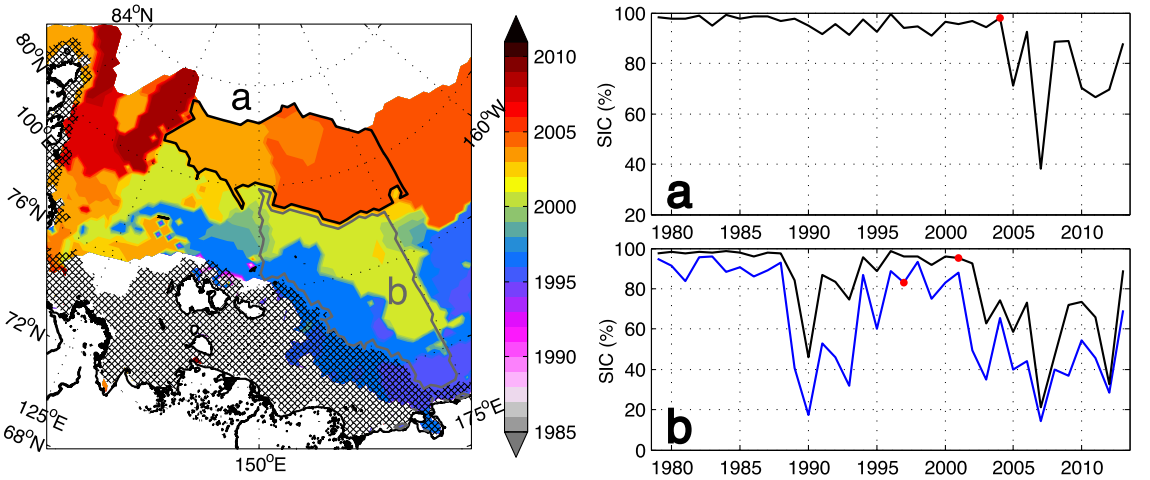

Figure 8. Map of summer transition times for Laptev and East Siberian Seas. Hatching indicates the presence of fast ice. Area mean time series are shown in Figures 8a and 8b for the two regions labeled on the map, with the two time series in Figure 8b showing the pre-1998 and post-1998 area means within the region (the blue line corresponds to the blue region, and the black line to the green/yellow region). Red points indicate the area mean breakpoints. Area a is outlined in black, and area b in grey on the map.

The time series of the East Siberian Sea, shown in Figure 8b, suggest an important role of low-frequency variability in this region, exhibiting low-frequency oscillatory behavior after ~1990. Considering the blue curve (corresponding to the near-coast region where the onset time is found in 1996) purely visually, it might be argued that there is some justification for suggesting that an initial transition occurs in 1987. Owing to the strong variability, the simplified time series created by the algorithm comprise a number of vertices (generally 4–6) in this region, and the earliest vertex indeed corresponds to this 1987 timing rather uniformly across the region. However, the algorithm selects 1996, since the greatest decrease in SIC is found between 1997 and 2007 (further, in the LOWESS-filtered time series, the magnitude of the oscillation between 1987 and 1994 is reduced, due to the recovery in SIC over 1994–2001). This leads to an onset time that is closer to that of the green/yellow region (onset time in 2001) lying to the north, where an event occurring between 1987 and 1994 is also evident, albeit with reduced magnitude and a stronger recovery of SIC afterward. Nevertheless, this interior region experiences an equally strong loss after 2001 to that of the more southerly region. The form of this loss is similar in the autumn over the wider green/yellow (2000/2001 onset time) region seen in Figure 3b, suggesting a transition to a lower mean state after ca. 2000. This timing is consistent with mooring results presented by *Woodgate et al.* [2010], which show an increase in annual mean oceanic heat transport through the Bering Strait that also begins in 2001 and may plausibly be reflected in this step change (see their Figure 2d).

In an analysis of sea ice motion from buoys, *Rigor et al.* [2002] linked high-index winter Arctic Oscillation (AO) conditions to increased export of ice from the East Siberian and Laptev Seas, leading to increased divergence over the eastern Arctic and a thinning of the ice; they postulate that the winter AO preconditions the summer ice via the ice thickness, leading to a seasonally lagged correlation between the two. The onset time and low-frequency variability associated with the East Siberian Sea region here is consistent with this suggestion of a link between the summer sea ice and the AO of the preceding winter, which switched from a positive state (in an oscillation beginning ca. 1989) to neutral/negative conditions in approximately 1996. The detrended time series for the near-coastal region (blue line in Figure 8b) is indeed significantly correlated with the DJF mean AO ($r=-0.61$). However, the correlation with the northerly (yellow, 2002 onset) region, shown by the black time series in Figure 8b is not significant, even after detrending ($r=-0.41$). Further investigation of the relationship between these two time series and the winter AO, using a 10 year sliding window to calculate the correlations, reveals that the correlation is localized in time, being significant only in the first part of the time series (the correlation declines sharply after 1996, but also becomes marginally significant again after 2006). This suggests that the primary influence of the AO is limited spatially to the outer region (where the initial coverage over 1979–1987 is slightly weaker and the variance greater than for the inner region, indicating that the SIC in this region might be more susceptible to external forcing) and also temporally to periods when the AO is relatively strong.

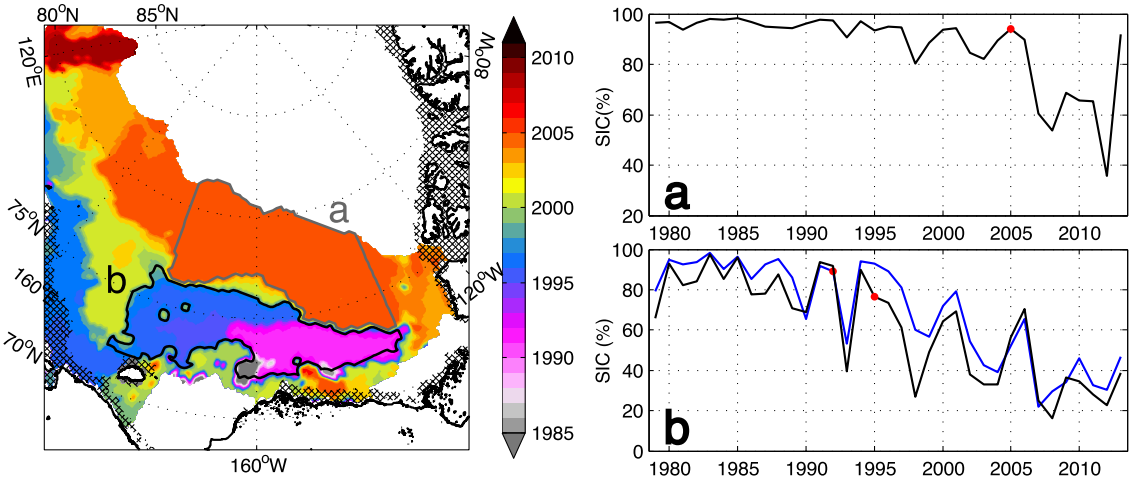

Figure 9. Map of summer transition times for the Bering Strait and Beaufort Sea and north Alaskan coastal region. Hatching indicates the presence of fast ice. Area mean time series are shown in Figures 9a and 9b for the two regions labeled on the map, with the two time series in Figure 9b showing the pre-1994 and post-1994 area means within the region (corresponding to the western and eastern sections of region b. The blue line corresponds to the blue region, and the black line to the pink region). Red points indicate the area mean breakpoints. Area a is outlined in grey, and area b in black on the map.

4.3. Chukchi and Beaufort Seas and Alaskan Coast

As noted above, the northern region of the domain, where the onset year occurs in 2005 (Figure 9a), is coherent with the region highlighted in Figure 8a for the East Siberian sector. It is hypothesized that this region of 2005 onset may reflect the exceptional SIC minimum that occurred in 2007 (since the onset time marks the point at which the decline begins, and thus for a step change is the final "peak" year having conditions associated with the prestep state). In contrast with the 2012 minimum that was particularly pronounced in the Atlantic sector, the 2007 minimum had a particularly strong impact on SIC in the Pacific sector. The exceptional conditions of 2007 have been widely discussed in the literature, with increased solar heating and associated ice-albedo feedback [*Perovich et al.*, 2008], anomalously high transport of heat through the Bering Strait [*Woodgate et al.*, 2010], and continued thinning of the ice [*Lindsay et al.*, 2009] in association with exceptional atmospheric forcing, driving increased ice motion [*Maslanik et al.*, 2007] all being implicated in the large-scale conditions. The 2007 minimum is an exceptionally low value of SIC in the time series of Figure 9a, and the ice does not recover to its preonset mean state after this event, with a decline of ca. 20% in the mean value, representing a transition to partial coverage (cf. Figure 4e).

At a regional level, further mechanisms may have played a role in driving local conditions in the 2007 minimum. In the Beaufort Sea, *Hutchings and Rigor* [2012] find ice drift to play an important role in preconditioning the ice pack, and thus influencing the 2007 event. They further note the presence of an unusual polynya in the Beaufort Sea in 2006, and suggest that both events are linked to the reduced replenishment of multiyear ice over most of the Beaufort Sea region. This timing is thus consistent with the 2005/2006 onset years found in this work for the inner transition band of the summer, and suggests a role of both dynamical and thermodynamical forcing in the ice decline.

Contrasting with the previously described regimes of sudden rapid ice loss, the region spanning the Alaskan coast between the Chukchi and Beaufort Seas (transition years in 1992/1995 at the respective western and eastern ends of the region, Figure 9b) are characterized by a much slower, long-term decline that begins early in the time series, with relatively large amplitude interannual variability superimposed on this continuous, but weaker trend, and a strong increase in variability after the onset of the trend. The forms of the time series for the western and eastern ends of this region are nearly identical, both in the magnitude of the trend and its interannual variability. (The later onset time detected in the western part of the region is due to the stronger decline experienced there in 1998, leading to a weaker trend over the 1998–2013 period here relative to that of the eastern side of the region.) In summer, following the onset of decline, the SIC in this region decreases approximately linearly until the end of the period, with a trend of ~2.6%/yr ($r^2 = 0.41$). The trend is little changed if the entire time series is considered (~2.2%/yr, $r^2 = 0.64$), suggesting that this region may be responding to ongoing forcing. In contrast, in autumn, both the spatial extent of this region (see Figure 3b)

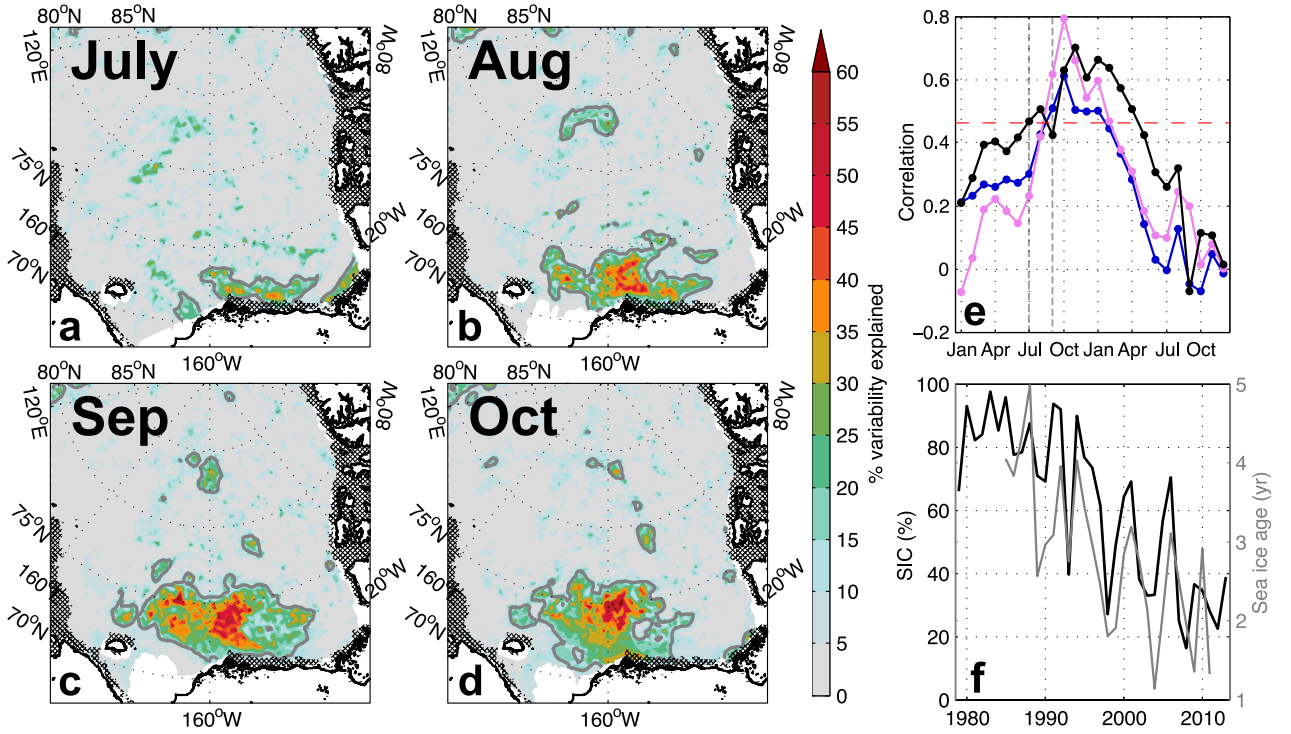

Figure 10. (a–d) Lagged correlation of ice age with summer (JAS) SIC averaged over region b of Figure 9. Hatching indicates the presence of fast ice and grey contours indicate regions where the correlation is significant at the 95% level. (e) Lagged correlation between mean ice age in region b and mean SIC in the region (the blue line corresponds to the blue region, the pink line to the pink region and the black line to the whole region. Grey dashed lines indicate the bounds within which the two time series are in phase and the red line shows the 95% significance level). (f) Time series of SIC (black line) and ice age (grey line) averaged over region b.

and the rate of decline are greatly reduced, corresponding to a loss of only 0.33%/yr. Motivated by the similar onset time found in this region to the outer edge of the East Siberian Sea (the blue part of region b in Figure 8), and the apparent convergence of these two regions adjacent to Wrangel Island, their area mean time series have been compared; however, the two are not significantly correlated. Despite the similar onset times, the two regions thus appear to be associated with different dynamics.

Regarding the early (1992/1995) onset region found spanning the Alaskan coast and Chukchi Sea, there are no clear indications from the literature as to with what this onset might coincide. However, comparison with ice thickness fields from the Pan-Arctic Ice Ocean Modeling and Assimilation System [*Zhang and Rothrock*, 2003] suggests that, in the model, the decrease in SIC occurs coincidentally with a decrease in ice thickness. Indeed, the transition time of 1992 is comparable with the value of 1987 suggested by *Lindsay et al.* [2009] as the start time for the decline in ice thickness at an Arctic-wide scale. The region corresponds to a pathway of advection of multiyear ice away from the area north of the Canadian Arctic Archipelago [e.g., *Kwok and Cunningham*, 2010; *Comiso*, 2012], and indeed, several features in the time series shown in Figure 9b correspond to events noted in the multiyear ice record (such as the minimum in 2007/2008 noted by *Kwok and Cunningham* [2010]). Comparison with the maps of change in albedo and absorbed solar radiation presented by *Perovich et al.* [2011] and *Stroeve et al.* [2014] further shows this area to be colocated with a maximum in annual solar heat input and its trend [see *Perovich et al.*, 2011, Figures 1 and 3] and also with the strongest reduction in albedo over the Arctic region [see *Stroeve et al.*, 2014, Figure 3a]. However, it is difficult to separate cause and effect in these relationships, since declining SIC, reductions in albedo, increased capacity to absorb solar radiation and changes in ice velocity are all interdependent.

We hypothesize that it is the presence of multiyear ice that is responsible for the very different signature of the early onset region with respect to the surrounding area. Regression of the monthly MEaSUREs Arctic Sea Ice Characterization ice age fields [*Anderson et al.*, 2014] on to the summer SIC time series averaged over region b of Figure 9 shows the development and propagation of a significantly correlated pattern away from the Canadian Arctic Archipelago and Alaskan coast and into a region corresponding to that where the early onset years occur in our estimates of transition time (Figures 10a–10d). The correlation for the immediately

preceding/following months becomes significant in August, and persists until the following February (Figure 10e), with the area mean time series of summer ice age and summer SIC for region b being correlated with $r = 0.86$ prior to detrending (linearly, over the full common available period of 1985–2011), and $r = 0.81$ afterward. The time series for this region in summer are furthermore significantly correlated with the westward ice velocity in this region in the preceding spring: the ice velocity explains approximately 50% of the sea ice variability (not shown). These results thus suggest that the form of decline of this anomalous region of early onset may be linked to the amount of multiyear ice imported to the region from the Canadian Arctic Archipelago, with the decline in SIC corresponding to a decrease in ice age. While estimates of ice age are only available after 1985, making it impossible to assess whether the decline of the two time series shown in Figure 10f begins at the same time, over the available record the forms of the time series coincide.

5. Summary and Conclusions

The onset of rapid loss in Arctic sea ice has been examined on a regional basis, using an objective method based on the point-wise application of the Ramer-Douglas-Peucker algorithm. For wide regions of the Arctic, the form of the ice loss at a given location can be described as a transition between two different states, preonset and postonset, where there is either a significant change in rate of change of SIC between the two periods or a significant change in the mean state of the SIC. Approximately 70% of the ice-covered Arctic in summer, and approximately 50% of the ice-covered Arctic in autumn can be described using this model based on the notion of a breakpoint (i.e., a transition in the state of the ice). The sea ice cover is found to be much more stable in winter and spring than in summer and autumn, with breakpoints being found only in a few localized regions. The onset times found in winter and spring are compatible with those found in the same regions in summer and autumn, leading to a focus here on the latter two seasons.

The maps of onset time presented in this work suggest that there is a strong regionality inherent in recent decreases in Arctic sea ice concentration. A demarcation can be drawn between the recent onset times found in the Barents Sea (ca. 2003/2004) and Nansen Basin (post-2008), and those associated with the Pacific sector of the Arctic, where, in summer, the decline in certain regions begins as early as 1992; our results thus highlight a difference in onset time of up to 20 years between the various Arctic subregions. Further, even at the much smaller scale of the individual seas of the Arctic Ocean, the physical behavior of the ice cannot be assumed to be uniform based on simple geographical definitions (see e.g., the Laptev Sea, Figure 8). These results suggest that areas that are frequently grouped together in regional studies using geographically defined criteria may not have physically coherent behavior. As an example, in the definitions of *Parkinson et al.* [1999], which are widely used and are those adopted by the NSIDC, the "Arctic Ocean" comprises regions that span the 20 year difference noted above. Given the strongly differing forms of the time series of SIC noted here, it appears that such an area mean cannot be assumed to be representative of the individual regions that comprise it, particularly at interdecadal time scales.

Consistent with previous estimates of full-period rates of decline based on simple linear regression, we find that the posttransition rates of sea ice loss are greatest in the Barents Sea. Where breakpoints occur at the same location in different seasons, over wide areas of the Arctic, the onset timing is found to be coherent between these seasons. Where this is not the case, a later breakpoint is found in autumn than in summer, and reflects the stronger sea ice coverage in autumn, which appears to be able to better withstand the interannual forcing. However, the interannual variability between summer and autumn around the trend is generally found to be coherent.

The form of the time series of SIC varies between regions. Broadly, the Barents and Kara Seas and a band spanning the interior of the Arctic Ocean between Fram Strait and the Beaufort Sea (via the eastern Arctic) may be characterized by a significant change in gradient between the preonset and postonset time. In contrast, the East Siberian Sea experiences strong low-frequency variability that appears to dominate the interannual-scale variability, while the Beaufort Sea/Alaskan coastline experiences a slow decline in SIC following an early transition, with strong interannual variability superimposed on this trend.

Comparison with the literature suggests that the results found in this work are broadly consistent with existing regional studies investigating SIC forcing mechanisms and the numerous processes that have been implicated therein in recent sea ice decline. While large-scale influences such as increased radiative forcing may play a strong influence in determining the long-term decrease, we suggest that additional, regional-scale differences are also an important factor in the onset of rapid decline. The maps presented here may thus be of use in

understanding the sensitivities of SIC in different regions. Finally, for studies concerned with pan-Arctic estimates of ice properties, these results suggest that care should be taken in the definition of any "cutoff-thresholds" for transitions in behavior, which may be misaligned with the regional-scale response.

Acknowledgments
The research leading to these results has received funding from the European Union 7th Framework Programme (FP7 2007–2013) under grant 308299, NACLIM Project. All sea ice data sets used in this work are available from the National Snow and Ice Data Center (http://nsidc.org/data). ERA interim reanalysis data are made available by the European Centre for Medium-range Weather Forecasting (http://apps.ecmwf.int/datasets/) and the EN4 data set by the UK Met Office (http://hadobs.metoffice.com/en4/index.html). This work has benefited from discussions during FAMOS meetings and support from the FAMOS project. We are grateful to two anonymous reviewers for their helpful comments on the manuscript.

References

Alexeev, V. A., V. V. Ivanov, R. Kwok, and L. H. Smedsrud (2013), North Atlantic warming and declining volume of arctic sea ice, *Cryosphere Discuss.*, *7*(1), 245–265, doi:10.5194/tcd-7-245-2013.

Anderson, M. R., A. C. Bliss, and M. Tschudi (2014), MEaSUREs Arctic Sea ice characterization daily 25 km EASE-Grid 2.0, [1979–2012], technical report, NASA DAAC at the Natl. Snow and Ice Data Cent., Boulder, Colo., doi:10.5067/MEASURES/CRYOSPHERE/nsidc-0532.001.

Årthun, M., T. Eldevik, L. H. Smedsrud, Ø. Skagseth, and R. B. Ingvaldsen (2012), Quantifying the influence of Atlantic Heat on Barents Sea Ice variability and retreat, *J. Clim.*, *25*(13), 4736–4743, doi:10.1175/JCLI-D-11-00466.1.

Boyer, T., et al. (2013), World Ocean Database 2013, *NOAA Atlas NESDIS 72*, edited by S. Levitus, 209 pp., National Oceanic and Atmospheric Administration, Silver Spring, Md., doi:10.7289/V5NZ85MT.

Cavalieri, D. J., and C. L. Parkinson (2012), Arctic sea ice variability and trends, 1979–2010, *Cryosphere*, *6*(4), 881–889, doi:10.5194/tc-6-881-2012.

Cleveland, W. S. (1979), Robust locally weighted regression and smoothing scatterplots, *J. Am. Stat. Assoc.*, *74*(368), 829–836, doi:10.1080/01621459.1979.10481038.

Comiso, J. C. (2000), *Bootstrap Sea Ice Concentrations From Nimbus-7 SMMR and DMSP SSM/I-SSMIS. Version 2*, doi:10.5067/J6JQLS9EJ5HU.

Comiso, J. C. (2012), Large decadal decline of the Arctic multiyear ice cover, *J. Clim.*, *25*(4), 1176–1193, doi:10.1175/JCLI-D-11-00113.1.

Day, J. J., J. C. Hargreaves, J. D. Annan, and A. Abe-Ouchi (2012), Sources of multi-decadal variability in Arctic sea ice extent, *Environ. Res. Lett.*, *7*(3), 034011.

Dee, D. P., et al. (2011), The ERA-Interim reanalysis: Configuration and performance of the data assimilation system, *Q. J. R. Meteorol. Soc.*, *137*(656), 553–597, doi:10.1002/qj.828.

Deser, C., and H. Teng (2008), Evolution of Arctic sea ice concentration trends and the role of atmospheric circulation forcing, 1979–2007, *Geophys. Res. Lett.*, *35*, L02504, doi:10.1029/2007GL032023.

Dmitrenko, I. A., I. V. Polyakov, S. A. Kirillov, L. A. Timokhov, I. E. Frolov, V. T. Sokolov, H. L. Simmons, V. V. Ivanov, and D. Walsh (2008), Toward a warmer Arctic Ocean: Spreading of the early 21st century Atlantic Water warm anomaly along the Eurasian Basin margins, *J. Geophys. Res.*, *113*, C05023, doi:10.1029/2007JC004158.

Douglas, D. H., and T. K. Peucker (1973), Algorithms for the reduction of the number of points required to represent a digitized line or its caricature, *Can. Cartogr.*, *10*(2), 112–122, doi:10.3138/FM57-6770-U75U-7727.

Eisenman, I., and J. S. Wettlaufer (2009), Nonlinear threshold behavior during the loss of Arctic sea ice, *Proc. Natl. Acad. Sci. U. S. A.*, *106*(1), 28–32, doi:10.1073/pnas.0806887106.

Fetterer, F. (2006), A selection of documentation related to National Ice Center sea ice charts in digital format, *NSIDC Spec. Rep. 13*, Natl. Snow and Ice Data Cent., Boulder, Colo.

Fowler, C., J. Maslanik, W. Emery, and M. Tschudi (2013), Polar Pathfinder Daily 25 km EASE-Grid Sea Ice Motion Vectors. Version 2, National Snow and Ice Data Center, Boulder, Colo.

Fetterer, F., and C. Fowler (2006), *National Ice Center Arctic Sea Ice Charts and Climatologies in Gridded Format*, Natl. Snow and Ice Data Cent., Boulder, Colo., doi:10.7265/N5X34VDB.

Giles, K. A., S. W. Laxon, and A. L. Ridout (2008), Circumpolar thinning of Arctic sea ice following the 2007 record ice extent minimum, *Geophys. Res. Lett.*, *35*, L22502, doi:10.1029/2008GL035710.

Good, S. A., M. J. Martin, and N. A. Rayner (2013), EN4: Quality controlled ocean temperature and salinity profiles and monthly objective analyses with uncertainty estimates, *J. Geophys. Res. Oceans*, *118*, 6704–6716, doi:10.1002/2013JC009067.

Haas, C., A. Pfaffling, S. Hendricks, L. Rabenstein, J.-L. Etienne, and I. Rigor (2008), Reduced ice thickness in Arctic transpolar drift favors rapid ice retreat, *Geophys. Res. Lett.*, *35*, L17501, doi:10.1029/2008GL034457.

Herbaut, C., M.-N. Houssais, S. Close, and A.-C. Blaizot (2015), Two wind-driven modes of winter sea ice variability in the Barents Sea, *Deep Sea Res., Part I*, *106*, 97–115, doi:10.1016/j.dsr.2015.10.005.

Holland, M. M., C. M. Bitz, and B. Tremblay (2006), Future abrupt reductions in the summer Arctic sea ice, *Geophys. Res. Lett.*, *33*, L23503, doi:10.1029/2006GL028024.

Hutchings, J. K., and I. G. Rigor (2012), Role of ice dynamics in anomalous ice conditions in the Beaufort Sea during 2006 and 2007, *J. Geophys. Res.*, *117*, C00E04, doi:10.1029/2011JC007182.

Karcher, M. J., R. Gerdes, F. Kauker, and C. Köberle (2003), Arctic warming: Evolution and spreading of the 1990s warm event in the Nordic seas and the Arctic Ocean, *J. Geophys. Res.*, *108*(C2), 3034, doi:10.1029/2001JC001265.

Kay, J. E., M. M. Holland, and A. Jahn (2011), Inter-annual to multi-decadal Arctic sea ice extent trends in a warming world, *Geophys. Res. Lett.*, *38*, L15708, doi:10.1029/2011GL048008.

Koenigk, T., U. Mikolajewicz, J. Jungclaus, and A. Kroll (2009), Sea ice in the Barents Sea: Seasonal to interannual variability and climate feedbacks in a global coupled model, *Clim. Dyn.*, *32*(7–8), 1119–1138, doi:10.1007/s00382-008-0450-2.

Krishfield, R. A., A. Proshutinsky, K. Tateyama, W. J. Williams, E. C. Carmack, F. A. McLaughlin, and M.-L. Timmermans (2014), Deterioration of perennial sea ice in the Beaufort Gyre from 2003 to 2012 and its impact on the oceanic freshwater cycle, *J. Geophys. Res. Oceans*, *119*, 1271–1305, doi:10.1002/2013JC008999.

Kwok, R. (2009), Outflow of Arctic Ocean Sea Ice into the Greenland and Barents Seas: 1979–2007, *J. Clim.*, *22*(9), 2438–2457, doi:10.1175/2008JCLI2819.1.

Kwok, R., and G. F. Cunningham (2010), Contribution of melt in the Beaufort Sea to the decline in Arctic multiyear sea ice coverage: 1993–2009, *Geophys. Res. Lett.*, *37*, L20501, doi:10.1029/2010GL044678.

Kwok, R., W. Maslowski, and S. W. Laxon (2005), On large outflows of Arctic sea ice into the Barents Sea, *Geophys. Res. Lett.*, *32*, L22503, doi:10.1029/2005GL024485.

Lindsay, R. W., and J. Zhang (2005), The thinning of Arctic Sea Ice, 1988–2003: Have we passed a tipping point?, *J. Clim.*, *18*(22), 4879–4894, doi:10.1175/JCLI3587.1.

Lindsay, R. W., J. Zhang, A. Schweiger, M. Steele, and H. Stern (2009), Arctic Sea Ice retreat in 2007 follows thinning trend, *J. Clim.*, *22*(1), 165–176, doi:10.1175/2008JCLI2521.1.

Livina, V. N., and T. M. Lenton (2013), A recent tipping point in the Arctic sea-ice cover: Abrupt and persistent increase in the seasonal cycle since 2007, *Cryosphere*, *7*(1), 275–286, doi:10.5194/tc-7-275-2013.
Maslanik, J. A., C. Fowler, J. Stroeve, S. Drobot, J. Zwally, D. Yi, and W. Emery (2007), A younger, thinner Arctic ice cover: Increased potential for rapid, extensive sea-ice loss, *Geophys. Res. Lett.*, *34*, L24501, doi:10.1029/2007GL032043.
Miles, M. W., D. V. Divine, T. Furevik, E. Jansen, M. Moros, and A. E. J. Ogilvie (2014), A signal of persistent Atlantic multidecadal variability in Arctic sea ice, *Geophys. Res. Lett.*, *41*, 463–469, doi:10.1002/2013GL058084.
Morison, J., R. Kwok, C. Peralta-Ferriz, M. Alkire, I. Rigor, R. Andersen, and M. Steele (2012), Changing Arctic Ocean freshwater pathways, *Nature*, *481*(7379), 66–70.
Onarheim, I., L. Smedsrud, R. Ingvaldsen, and F. Nilsen (2014), Loss of sea ice during winter north of Svalbard, *Tellus, Ser. A*, *66*, 23933, doi:10.3402/tellusa.v66.23933.
Overland, J., and M. Wang (2010), Large-scale atmospheric circulation changes are associated with the recent loss of Arctic sea ice, *Tellus, Ser. A*, *62*(1), 1–9.
Overland, J., M. Wang, and S. Salo (2008), The recent Arctic warm period, *Tellus, Ser. A*, *60*(4), 589–597.
Overland, J. E., J. A. Francis, E. Hanna, and M. Wang (2012), The recent shift in early summer Arctic atmospheric circulation, *Geophys. Res. Lett.*, *39*, L19804, doi:10.1029/2012GL053268.
Parkinson, C. L., and D. J. Cavalieri (2008), Arctic sea ice variability and trends, 1979–2006, *J. Geophys. Res.*, *113*, C07003, doi:10.1029/2007JC004558.
Parkinson, C. L., and J. C. Comiso (2013), On the 2012 record low Arctic sea ice cover: Combined impact of preconditioning and an August storm, *Geophys. Res. Lett.*, *40*, 1356–1361, doi:10.1002/grl.50349.
Parkinson, C. L., D. J. Cavalieri, P. Gloersen, H. J. Zwally, and J. C. Comiso (1999), Arctic sea ice extents, areas, and trends, 1978–1996, *J. Geophys. Res.*, *104*(C9), 20,837–20,856, doi:10.1029/1999JC900082.
Perovich, D., K. Jones, B. Light, H. Eicken, T. Markus, J. Stroeve, and R. Lindsay (2011), Solar partitioning in a changing Arctic sea-ice cover, *Ann. Glaciol.*, *52*(57), 192–196.
Perovich, D. K. (2011), The changing Arctic sea ice cover, *Oceanography*, *24*(3), 162–173, doi:10.5670/oceanog.2011.68.
Perovich, D. K., J. A. Richter-Menge, K. F. Jones, and B. Light (2008), Sunlight, water, and ice: Extreme Arctic sea ice melt during the summer of 2007, *Geophys. Res. Lett.*, *35*, L11501, doi:10.1029/2008GL034007.
Polyakov, I. V., et al. (2010), Arctic Ocean warming contributes to reduced polar ice cap, *J. Phys. Oceanogr.*, *40*(12), 2743–2756, doi:10.1175/2010JPO4339.1.
Polyakov, I. V., et al. (2011a), Fate of early 2000s Arctic warm water pulse, *Bull. Am. Meteorol. Soc.*, *92*(5), 561–566, doi:10.1175/2010BAMS2921.1.
Polyakov, I. V., A. V. Pnyushkov, R. Rember, V. V. Ivanov, Y. D. Lenn, L. Padman, and E. C. Carmack (2011b), Mooring-based observations of double-diffusive staircases over the Laptev sea slope, *J. Phys. Oceanogr.*, *42*(1), 95–109, doi:10.1175/2011JPO4606.1.
Polyakov, I. V., A. V. Pnyushkov, and L. A. Timokhov (2012), Warming of the intermediate Atlantic Water of the Arctic Ocean in the 2000s, *J. Clim.*, *25*(23), 8362–8370, doi:10.1175/JCLI-D-12-00266.1.
Quadfasel, D., A. Sy, D. Wells, and A. Tunik (1991), Warming in the Arctic, *Nature*, *350*(6317), 385–386.
Rabe, B., M. Karcher, F. Kauker, U. Schauer, J. M. Toole, R. A. Krishfield, S. Pisarev, T. Kikuchi, and J. Su (2014), Arctic Ocean basin liquid freshwater storage trend 1992–2012, *Geophys. Res. Lett.*, *41*, 961–968, doi:10.1002/2013GL058121.
Ramer, U. (1972), An iterative procedure for the polygonal approximation of plane curves, *Comput. Graphics Image Process.*, *1*(3), 244–256, doi:10.1016/S0146-664X(72)80017-0.
Rigor, I. G., and J. M. Wallace (2004), Variations in the age of Arctic sea-ice and summer sea-ice extent, *Geophys. Res. Lett.*, *31*, L09401, doi:10.1029/2004GL019492.
Rigor, I. G., J. M. Wallace, and R. L. Colony (2002), Response of sea ice to the Arctic Oscillation, *J. Clim.*, *15*(18), 2648–2663, doi:10.1175/1520-0442(2002)015 < 2648:ROSITT>2.0.CO;2.
Rodionov, S. N. (2004), A sequential algorithm for testing climate regime shifts, *Geophys. Res. Lett.*, *31*, L09204, doi:10.1029/2004GL019448.
Sandø, A. B., Y. Gao, and H. R. Langehaug (2014), Poleward ocean heat transports, sea ice processes, and Arctic sea ice variability in NorESM1-M simulations, *J. Geophys. Res. Oceans*, *119*, 2095–2108, doi:10.1002/2013JC009435.
Schauer, U., E. Fahrbach, S. Osterhus, and G. Rohardt (2004), Arctic warming through the Fram Strait: Oceanic heat transport from 3 years of measurements, *J. Geophys. Res.*, *109*, C06026, doi:10.1029/2003JC001823.
Schlichtholz, P. (2011), Influence of oceanic heat variability on sea ice anomalies in the Nordic Seas, *Geophys. Res. Lett.*, *38*, L05705, doi:10.1029/2010GL045894.
Serreze, M. C., M. M. Holland, and J. Stroeve (2007), Perspectives on the Arctic's shrinking sea-ice cover, *Science*, *315*(5818), 1533–1536, doi:10.1126/science.1139426.
Serreze, M. C., A. P. Barrett, J. C. Stroeve, D. N. Kindig, and M. M. Holland (2009), The emergence of surface-based Arctic amplification, *Cryosphere*, *3*(1), 11–19, doi:10.5194/tc-3-11-2009.
Simmonds, I., and I. Rudeva (2012), The great Arctic cyclone of August 2012, *Geophys. Res. Lett.*, *39*, L23709, doi:10.1029/2012GL054259.
Skagseth, Ø., T. Furevik, R. Ingvaldsen, H. Loeng, K. A. Mork, K. A. Orvik, and V. Ozhigin (2008), Volume and heat transports to the Arctic Ocean via the Norwegian and Barents Seas, in *Arctic-Subarctic Ocean Fluxes*, edited by R. R. Dickson, J. Meincke, and P. Rhines, chap. 2, pp. 45–64, Springer, Netherlands, doi:10.1007/978-1-4020-6774-7_3.
Spreen, G., L. Kaleschke, and G. Heygster (2008), Sea ice remote sensing using AMSR-E 89-GHz channels, *J. Geophys. Res.*, *113*, C02S03, doi:10.1029/2005JC003384.
Stroeve, J., M. Serreze, M. Holland, J. Kay, J. Malanik, and A. Barrett (2012), The Arctic's rapidly shrinking sea ice cover: A research synthesis, *Clim. Change*, *110*(3–4), 1005–1027, doi:10.1007/s10584-011-0101-1.
Stroeve, J. C., T. Markus, L. Boisvert, J. Miller, and A. Barrett (2014), Changes in Arctic melt season and implications for sea ice loss, *Geophys. Res. Lett.*, *41*, 1216–1225, doi:10.1002/2013GL058951.
Strong, C., and I. G. Rigor (2013), Arctic marginal ice zone trending wider in summer and narrower in winter, *Geophys. Res. Lett.*, *40*, 4864–4868, doi:10.1002/grl.50928.
Swart, N. C., J. C. Fyfe, E. Hawkins, J. E. Kay, and A. Jahn (2015), Influence of internal variability on Arctic sea-ice trends, *Nat. Clim. Change*, *5*(2), 86–89.
Tamura, T., K. I. Ohshima, T. Markus, D. J. Cavalieri, S. Nihashi, and N. Hirasawa (2007), Estimation of thin ice thickness and detection of fast ice from SSM/I data in the Antarctic Ocean, *J. Atmos. Oceanic Technol.*, *24*(10), 1757–1772, doi:10.1175/JTECH2113.1.
Tverberg, V., O. A. Nøst, C. Lydersen, and K. M. Kovacs (2014), Winter sea ice melting in the Atlantic Water subduction area, Svalbard Norway, *J. Geophys. Res. Oceans*, *119*, 5945–5967, doi:10.1002/2014JC010013.

Wessel, P., and W. H. F. Smith (1996), A global, self-consistent, hierarchical, high-resolution shoreline database, *J. Geophys. Res.*, *101*(B4), 8741–8743, doi:10.1029/96JB00104.

Woodgate, R. A., T. Weingartner, and R. Lindsay (2010), The 2007 Bering Strait oceanic heat flux and anomalous Arctic sea-ice retreat, *Geophys. Res. Lett.*, *37*, L01602, doi:10.1029/2009GL041621.

Yang, X.-Y., and X. Yuan (2014), The early winter sea ice variability under the recent Arctic climate shift, *J. Clim.*, *27*(13), 5092–5110, doi: 10.1175/JCLI-D-13-00536.1.

Yu, Y., H. Stern, C. Fowler, F. Fetterer, and J. Maslanik (2014), Interannual variability of Arctic landfast ice between 1976 and 2007, *J. Clim.*, *27*(1), 227–243, doi:10.1175/JCLI-D-13-00178.1.

Zhang, J., and D. A. Rothrock (2003), Modeling global sea ice with a thickness and enthalpy distribution model in generalized curvilinear coordinates, *Mon. Weather Rev.*, *131*(5), 845–861, doi:10.1175/1520-0493(2003)131 < 0845:MGSIWA>2.0.CO;2.

Zhang, J., R. Lindsay, A. Schweiger, and M. Steele (2013), The impact of an intense summer cyclone on 2012 Arctic sea ice retreat, *Geophys. Res. Lett.*, *40*, 720–726, doi:10.1002/grl.50190.

Zhang, R. (2015), Mechanisms for low-frequency variability of summer Arctic sea ice extent, *Proc. Natl. Acad. Sci. U. S. A.*, *112*(15), 4570–4575, doi:10.1073/pnas.1422296112.

Zhang, X., A. Sorteberg, J. Zhang, R. Gerdes, and J. C. Comiso (2008), Recent radical shifts of atmospheric circulations and rapid changes in Arctic climate system, *Geophys. Res. Lett.*, *35*, L22701, doi:10.1029/2008GL035607.